

**BLOCK THEORY APPLICATION TO SCOUR  
ASSESSMENT OF UNLINED ROCK SPILLWAYS**

by

**Michael F. George**

**Nicholas Sitar**

Report No. UCB GT 12-02



**GEOTECHNICAL ENGINEERING  
DEPARTMENT OF CIVIL AND ENVIRONMENTAL ENGINEERING  
UNIVERSITY OF CALIFORNIA • BERKELEY**

# Block Theory Application to Scour Assessment of Unlined Rock Spillways

---



by

Michael F. George  
Nicholas Sitar

Department of Civil & Environmental Engineering  
University of California  
Berkeley, California  
Report No. UCB GT 12-02

May 2012

---

## **Acknowledgements**

The research presented in this report was principally supported by a fellowship from the Hydro Research Foundation, with additional financial support provided by the University of California. PG&E generously permitted access to their field site and provided additional data which was not in public domain. Such commitment to this research is gratefully acknowledged.

This report is based on the CE299 Report “Scour of Discontinuous Blocky Rock” by Michael F. George (2012) submitted in partial satisfaction of the requirements for the degree of Master of Science and is part of an ongoing rock scour research study at the University of California – Berkeley.

---

## Summary

Scour of rock is a complex process and can be very problematic for dams when excessive scour threatens dam stability. Removal of individual rock blocks is one of the principal mechanisms by which scour can occur, particularly in unlined spillways and on dam abutments. Block removability is largely influenced by the 3D orientation of discontinuities within the rock mass, which current scour methods tend to ignore or simplify into 2D or cuboidal block geometries. To better represent the 3D structure of the rock mass, block theory (Goodman & Shi 1985) has been applied to identify removable blocks, determine potential failure modes, and assess block stability due to hydraulic loads.

Scour assessment was performed for representative size blocks (based on field investigations to determine average orientation and spacing of rock mass discontinuities) under representative hydraulic flow conditions. Depending on the turbulent nature of fluid motions in the vicinity of the rock mass being analyzed, stability of a block can be assessed in a simplified dynamic manner due to a single characteristic pressure impulse or in a more static sense through limit equilibrium methods (in the realm that block theory has traditionally been applied). The methodologies developed herein may be applied to any flow scenario as long as the characteristic hydrodynamic pressure is known.

Key to the analysis is the assumption of the distribution of hydrodynamic pressures on the block faces. In situations where flow conditions are complex and turbulent (such as plunge pools, rough channel flows with complex geometries, hydraulic jumps, etc.) it is logical to think that dynamic pressures may be distributed around the block in many different combinations that continually change over time. Therefore, hydrodynamic pressures can be assumed to be distributed uniformly over any combination of block faces. For tetrahedral blocks, this yields 15 load scenarios each of which is analyzed to determine the most critical load causing block removal. For static analysis, this number may be reduced to account for a preferential loading direction (such as flow in a channel).

Application of the methods was performed for an actively eroding unlined rock spillway at a dam site in northern California. Ten removable tetrahedral block types were identified from the channel bottom below the spillway gates. To assess stability, hydraulic pressures applied to the blocks were related to flow velocity based on a hydraulic jacking study from the USBR (2007). Accordingly, the critical flow velocity resulting in block removal could be identified, which for this analysis, ranged between 4.4 m/s and 11.9 m/s. Three of the removable blocks were stable over the entire range of anticipated flow velocities in the channel.

The variation of results show the influence on discontinuity orientation on block removability and the need to incorporate the full 3D structure of the rock mass when considering erodibility. Furthermore, determination of the critical hydraulic load was highly dependent on block shape and orientation of the block faces. As such, the minimum hydrodynamic pressure causing removal did not usually produce an active resultant path that was shortest in distance to the limit equilibrium contour line (in

---

the case of static analysis). Critical resultant paths were influenced by the relative size of the block faces, with the larger area controlling the direction of block removal.

Overall, the results show that more accurate predictions of scour are achievable as the site-specific 3D geologic structure is accounted for. Additionally, with detailed field mapping, blocks most susceptible to scour can be targeted such that more efficient remediation measures can be implemented thus potentially reducing costs. Finally, analyses may be used as a planning tool for future projects to determine the most optimal layout of new spillways, for example, that are least susceptible to scour.

---

# Table of Contents

Acknowledgements.....	i
Summary .....	ii
Table of Contents.....	iv
List of Tables .....	v
List of Figures .....	v
1. Introduction .....	1
2. Background .....	3
2.1 Scour Mechanisms .....	3
2.2 Existing Scour Prediction Methods .....	5
2.2.1 Limitations of Existing Scour Models .....	14
3. Methodology.....	15
3.1 Assumptions .....	15
3.2 Removability.....	15
3.3 Kinematic Mode Analysis .....	16
3.4 Stability.....	19
3.4.1 Characteristic Hydrodynamic Pressure.....	19
3.4.2 Hydrodynamic Pressure Distribution on Block.....	21
3.4.3 Pseudo-Static Block Stability.....	21
3.4.4 Dynamic Block Stability.....	24
4. Results (Case Study).....	27
4.1 Project Background .....	27
4.2 Field Investigations.....	29
4.3 Scour Assessment using Block Theory .....	31
4.3.1 Removability .....	32
4.3.2 Stability .....	32
5. Conclusions .....	37
5.1 Rock Mass Geometry .....	37
5.2 Flow Conditions.....	37
5.3 Hydrodynamic Pressure Distribution on Block .....	37
5.4 Block Stability .....	38
5.5 Implications .....	39
6. Recommendations for Further Study .....	40
7. References.....	42
Appendix A: Additional results and calculations .....	45

---

## List of Tables

Table 1: Summary of joint data used for block theory analysis. ....	30
Table 2: Block stability results summary. ....	35

## List of Figures

Figure 1: Scour from kinematic sliding failure of large rock blocks at Ricobayo Dam (Jan. & Mar. 1934).....	2
Figure 2: Scour remediation at Ricobayo (note extensive excavation and concrete work in addition to flow splitters on the spillway lip to dissipate hydraulic energy). ....	2
Figure 3: Fracture of intact rock. ....	3
Figure 4: Block removal. ....	4
Figure 5: Kinematic block failure modes (Goodman 1995). ....	5
Figure 6: Annandale Erodibility Index graph. ....	6
Figure 7: Key components of the CSM (Bollaert 2002). ....	7
Figure 8: Bollaert block removal model. ....	8
Figure 9: Non-dimensionalized power spectral density vs. frequency curve for pressure measurements at the top and bottom of a 3D cubic block. Note decline after approximately 10 Hz (Federspiel et al. 2009). ....	9
Figure 10: Analysis of abutment block due to overtopping jet impact (George & Annandale 2006).....	10
Figure 11: Hydraulic jacking of concrete spillway slabs (USBR, 2007) ....	11
Figure 12: Block uplift at bridge pier (Bollaert 2010). ....	12
Figure 13: 2D removable blocks in unlined spillway (Wibowo 2009). ....	13
Figure 14: Numerical simulation of plunge pool scour (Dasgupta et al. 2011).....	14
Figure 15: Upper hemisphere stereonet showing JP codes and removable blocks for horizontal free face (left) and vertical free face striking East-West (right). ....	16
Figure 16: Characteristic dynamic pressure. ....	19
Figure 17: Simplification of characteristic dynamic pressure for pseudo-static (top) & dynamic (bottom) analyses. ....	20
Figure 18: Example of vector solution for a removable block with hydraulic load applied to block face J3 and when applied to faces J2-J3. ....	23
Figure 19: Example of limit equilibrium stereonet for removable block showing resultant paths for hydraulic load applied to block face J3 and J2-J3 (stereonet generated with PanTechnica (2002) software). ....	24
Figure 20: Canyon formed by scour showing spillway gates in background (left). Approximately 2,000 cfs discharge in June 2010 (right). ....	28
Figure 21: Aerial view of spillway showing alluvial fan of eroded material (note the walkway across the primary spillway is approximately 300 ft long for scale). ....	28
Figure 22: Scan-line survey and block mold locations (left), NE striking scan-line survey (upper right), block mold below spillway gate (lower right). ....	29
Figure 23: Aerial LiDAR point cloud of primary spillway (left), and stereographic projection of joint normal orientations from LiDAR data (right). ....	30
Figure 24: Stereographic projection of hand-measured joint data (plotted in OpenStereo (Grohmann and Campanha 2011). ....	31

---

Figure 25: Simplified spillway schematic.....	31
Figure 26: Stereonet showing removable block for joint group containing J1, J2, J3, and $f$ .....	32
Figure 27: Limitation of active resultant paths for removable blocks (left) due to dominant flow direction in the spillway channel (right). ....	33
Figure 28: Stability of most critical removable block from spillway channel. ....	34
Figure 29: Example of block geometry dictating importance of pressure fluctuations for block removal.....	41

---

# 1. Introduction

Scour of rock is a critical issue facing many of the world's dams, with increasing safety concerns arising from the continued development of downstream communities. Excessive scour of the dam foundation or spillway can compromise the stability of the dam leading to high remediation costs and even the loss of life should catastrophic failure occur.

In the US, the application of more stringent requirements for managing the probable maximum flood (PMF), coupled with improved hydrologic methods and more robust climate data sets, has generally resulted in significantly greater estimated magnitudes of the design floods (Achterberg et al. 1998). Accordingly, the risk of foundation or spillway erosion is increased, particularly at existing structures that may now be inadequate to safely pass the revised design flow. Therefore, reliable prediction of scour for retrofit and new projects alike is vitally important.

Scour of rock is a complex process where removal of individual rock blocks is one of the principal mechanisms by which scour can occur, particularly in unlined spillways and on dam abutments. To alleviate some of the complexity, commonly used methods for scour prediction tend to simplify the rock mass using rectangular block geometries or incorporate empirical relationships for the rock mass and do not actually model the physical scour process. Such simplifications can be problematic, particularly for block analysis, where the 3D orientation of discontinuities within the rock mass largely influence block removability.

Furthermore, very little consideration has been given to the potential for the kinematic sliding or rotation failure of rock blocks when subject to impinging or overland flows. Failure of such blocks has been known to occur at discharges that are a fraction of the design discharge causing significant damage, but has still yet to be studied in-depth. Such a case is Ricobayo Dam in Spain that had a 400 m long unlined rock spillway with a capacity of 4,650 m<sup>3</sup>/s designed to discharge over a granite cliff. Within two years of operation, two separate events (with discharge of approximately 100 m<sup>3</sup>/s and 400 m<sup>3</sup>/s, respectively) resulted in the sliding failure of multiple rock blocks in the spillway (Figure 1). While the dam stability was not immediately threatened, significant cost was expended to contain and eventually remediate the scour (Figure 2).

A more rigorous approach to 3D characterization of the structure of the rock mass can be obtained using block theory (Goodman & Shi 1985). Block theory provides a methodology to identify removable blocks, determine potential failure modes, and assess block stability. The scour process is inherently dynamic while block theory is best suited for static conditions. There are, however, scenarios in which hydraulic loads may be considered in a pseudo-static sense or in a simplified dynamic sense such that the full power of block theory can be realized in a manner that is approachable in practice.

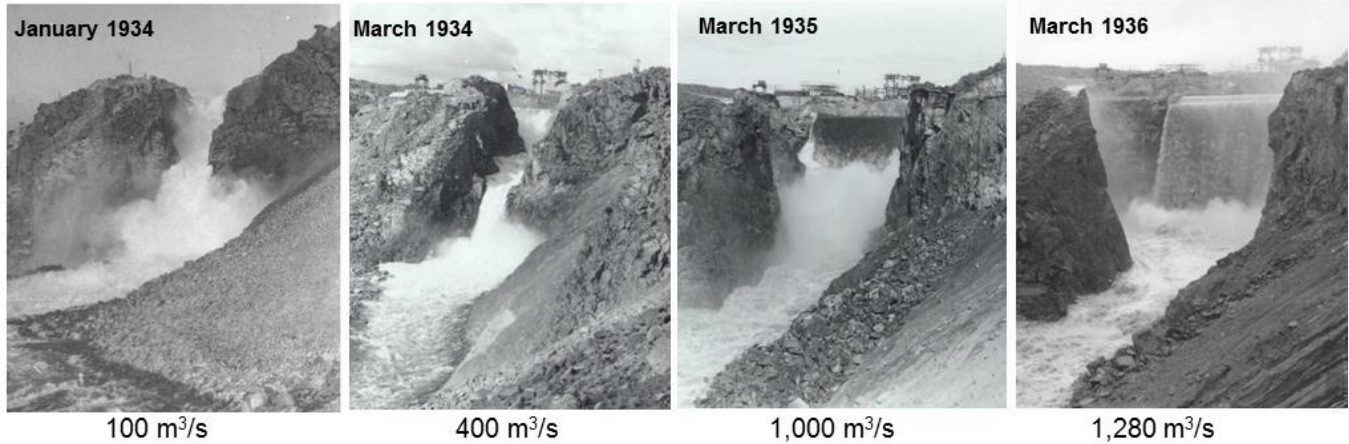


Figure 1: Scour from kinematic sliding failure of large rock blocks at Ricobayo Dam (Jan. & Mar. 1934).

Subsequently, the focus of this research has been to develop a framework within which block theory can be applied to evaluate the scour potential of 3D rock blocks in a more realistic and site-specific manner. Doing so may lead to more efficient (and less costly) remediation designs, improved tools for evaluating the optimal location and performance of future structures subject to scour, and more reliable (safe) infrastructure.

Methodologies developed herein have been applied to a case study for an actively eroding unlined rock spillway at a dam site in northern California.



Figure 2: Scour remediation at Ricobayo (note extensive excavation and concrete work in addition to flow splitters on the spillway lip to dissipate hydraulic energy).

---

## 2. Background

Numerous methods are available for prediction of scour for many types of flow conditions. This section is not meant to provide a review of every one, but rather discuss some of those more commonly used or those which focus on the removal of rock blocks. First, however, a discussion of the physical mechanisms leading to the break-up of a rock mass subject to hydraulic loads is presented.

### 2.1 Scour Mechanisms

The scour of rock can occur by three main mechanisms:

- Abrasion (ball-milling)
- Fracture of intact rock
- Removal in individual rock blocks

Abrasion, sometimes referred to as ball-milling, refers to the gradual grinding away of a rock surface due to repeated impacts from other particles (e.g., sand, cobbles, etc) carried by flowing water. Typically, the timescale for significant scour to occur by abrasion is generally very long (i.e., on a geomorphological timescale). As such, it is usually not a consideration for dam overtopping or spillway erodibility assessments.

Fracture of intact rock refers to the propagation (growth) of close-ended fissures when subject to hydraulic loads (Figure 3). This mechanism has been shown to be prominent at certain depths in plunge pools where conditions are such that resonance can lead to amplification of pressure within a rock fissure causing fracture of intact rock at the fissure tip (Bollaert 2002). Depending on the magnitude of the applied pressure, rock may fail nearly instantaneously by brittle fracture or over time by fatigue.

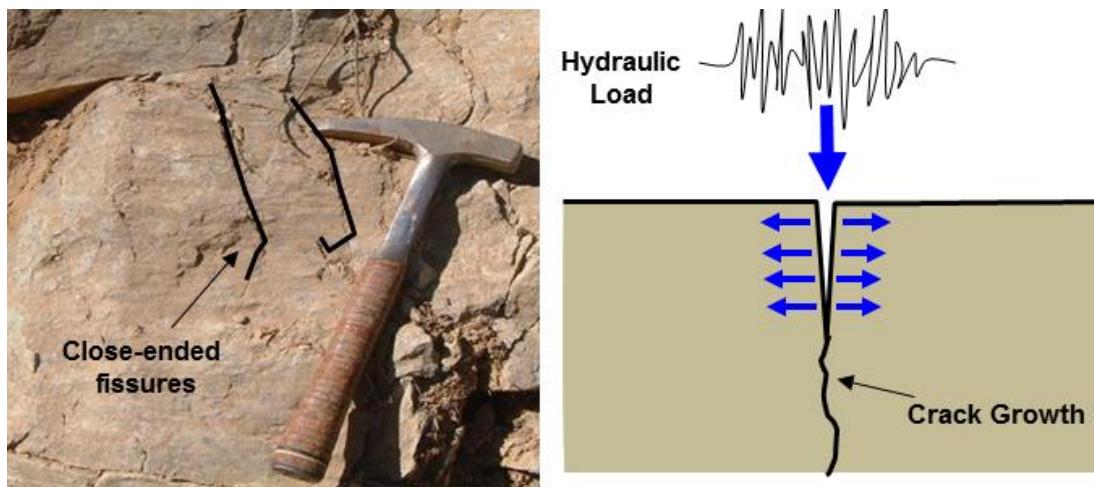


Figure 3: Fracture of intact rock.

---

Block removal refers to the “plucking” or “quarrying” of rock blocks from the surrounding rock mass due to forces induced by flowing water and gravity (Figure 4). Discontinuities bounding the blocks (such as joint planes, foliation, faults, contacts between geologic units or those created through brittle fracture / fatigue) allow for the transmission of transient water pressures to the underside of the block resulting in removal. Block removal is generally predominant when resonance conditions within rock joints / fissures cannot be achieved such that brittle fracture or fatigue failure does not significantly occur. Such scenarios may include direct flow impact onto a rock face (such as an overtopping jet plunging onto an abutment) or in unlined spillway channels.

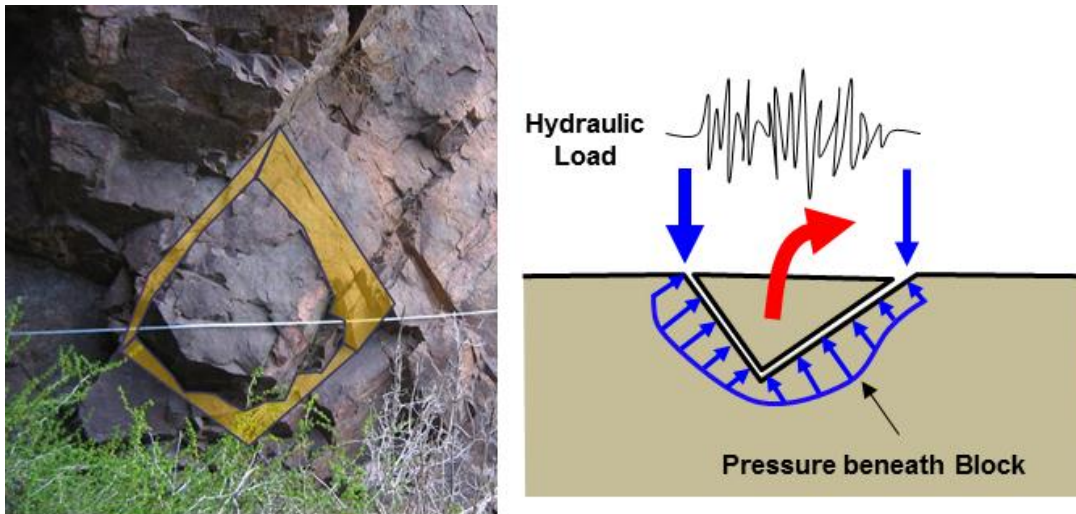


Figure 4: Block removal.

The removal of individual blocks from a rock mass is highly dependent on the 3D orientation of the discontinuities bounding the block, and subsequently, a number of kinematic failure modes exist (Figure 5).

Of these failure modes, lifting and sliding (1-plane or 2-plane) are pure translations meaning the resultant vector of all the forces applied to the rock block passes through the block centroid causing a zero moment about the centroid. Rotations about an edge or corner of the block are pure rotations where the resultant vector only acts along the axis of rotation. Combinations of translation and rotation can occur resulting in the slumping or torsional sliding of a block. Finally, flutter (not shown) may also occur when a block is subjected to a dynamic load such that small plastic displacements are realized over time and the block “walks” or “flutters” out of its mold. Note that a block mold refers to the space in the rock mass from which a block was removed.

It should be noted that for the above failure modes, blocks are assumed to be rigid. Block compressibility is more important for situations of combined rotation and translation where a significant moment about the block centroid exists (Tonon 2007, Asadollahi 2009).

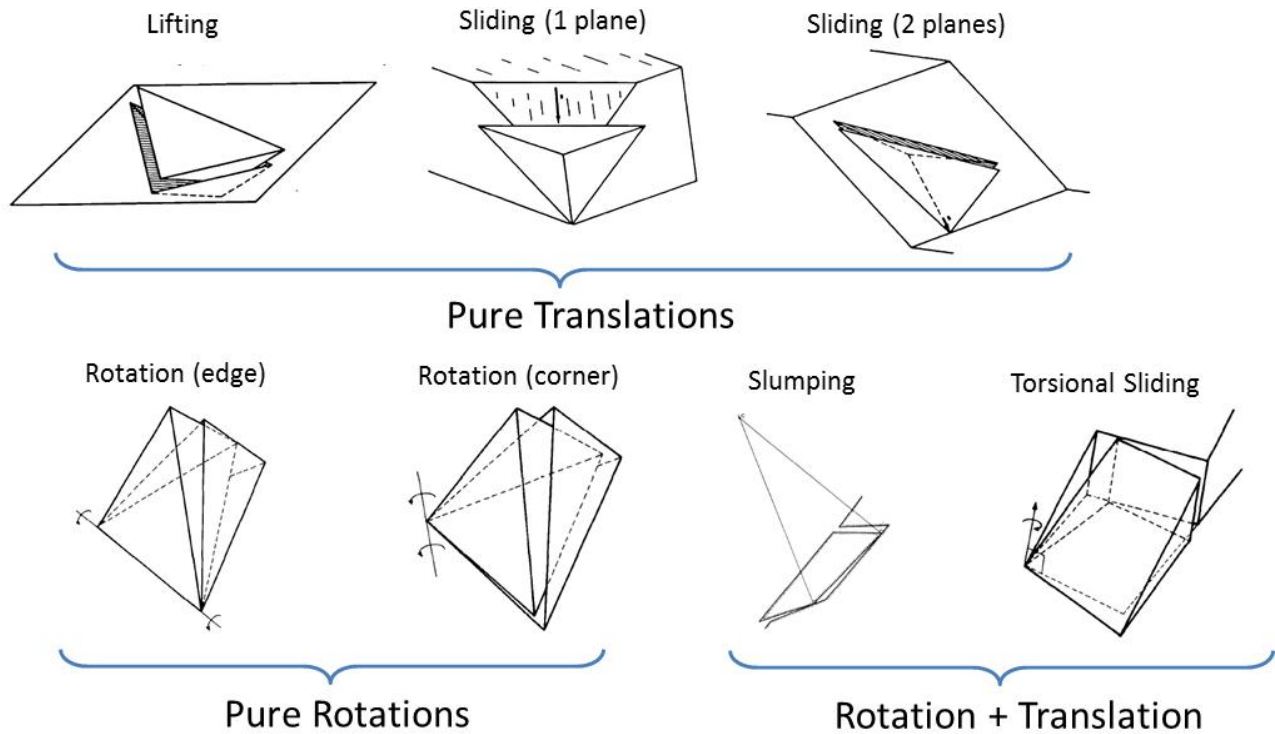


Figure 5: Kinematic block failure modes (Goodman 1995).

Due to the variety of flow conditions typically encountered in unlined channels, on dam abutments or in plunge pools, and the transient nature of pressure distributions on the various block faces, the potential for block removal in any of the above manners is likely high. Subsequently, methodologies for analyzing scour of rock blocks should consider these failure modes.

## 2.2 Existing Scour Prediction Methods

One of the most prominent methodologies for predicting rock scour is the Erodibility Index Method (EIM) from Annandale (1995, 2006). The EIM is a semi-empirical, geo-mechanical index that can be used to calculate the erosion resistance of any earth material (e.g., clay, sand, rock and even vegetation). The Erodibility Index,  $K$  (dimensionless), for rock is defined by:

$$K = M_s \cdot K_b \cdot K_d \cdot J_s \quad (1)$$

where:  $M_s$  = mass strength number (based on rock unconfined compressive strength (UCS)),  $K_b$  = block size number (based on rock quality designation (RQD) and number of discontinuity sets),  $K_d$  = discontinuity shear strength number (based on joint roughness and alteration), and  $J_s$  = relative ground structure number (based on strike and dip of discontinuities relative the flow direction).

Rock erodibility is based on a rippability index developed by Kirsten (1982, 1988) to evaluate the machine power required to excavate various earth materials. The index was modified from Barton’s Q-system used to classify rock masses for tunnel support (Barton et al. 1974, and Barton 1988).

To determine scour potential, rock erodibility is compared to the erosive capacity of water quantified using unit stream power,  $P_{sp}$  (expressed in  $W/m^2$ ). In general form, this may be expressed as:

$$P_{sp} = \frac{\gamma \cdot Q \cdot \Delta E}{A} \tag{2}$$

Where:  $\gamma$  = unit weight of water ( $N/m^3$ ),  $Q$  = the flow rate ( $m^3/s$ ),  $A$  = flow area ( $m^2$ ), and  $\Delta E$  = energy dissipated over the flow area, expressed in terms of hydraulic head (m).

Annandale (1995, 2006) provides modifications of the above equation to determine the erosive capacity for a variety of flow conditions including open channels, knick-points, hydraulic jumps, head-cuts and plunge pools. Based on 137 case studies and near-prototype hydraulic testing, Annandale developed a threshold relationship between flow erosive capacity and earth material erodibility (Figure 6). When the unit stream power of the water and the rock erodibility index plot above the threshold line, scour is likely to occur.

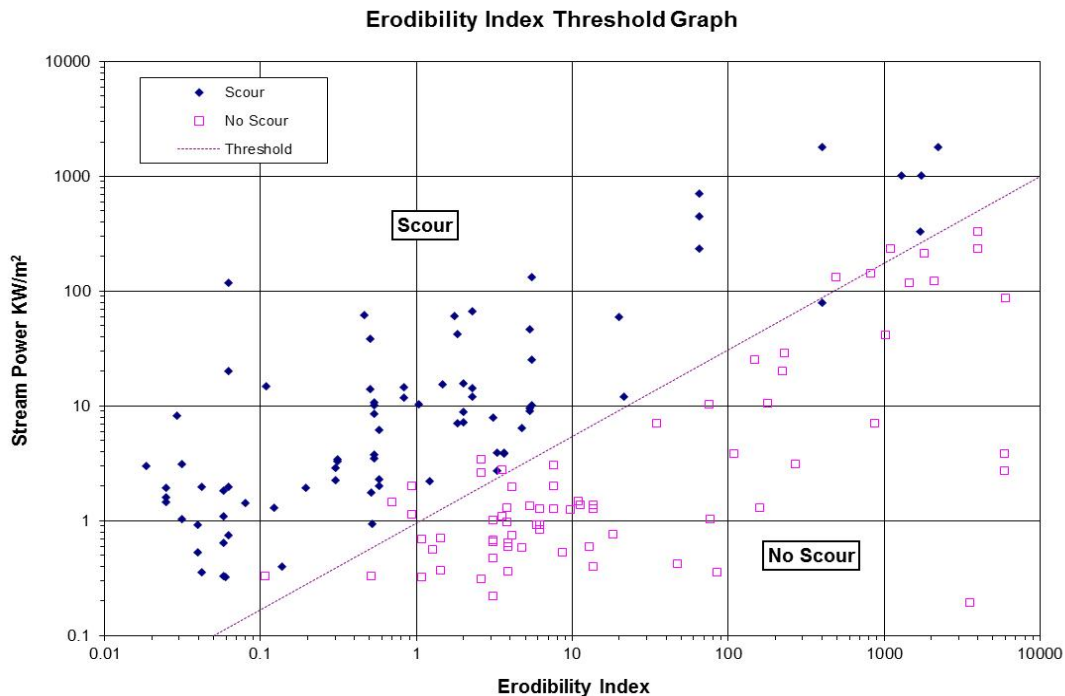


Figure 6: Annandale Erodibility Index graph.

The simplicity and wide applicability to various flow conditions makes the EIM particularly attractive for use in practice. The method, however, is not without limitation. As its name implies, the method incorporates an empirical index to characterize the rock. Subsequently, the EIM does not delineate between different scour mechanisms (i.e., brittle fracture, fatigue failure, or block removal). This results in a more generalized assessment of scour. Although weaker rock units or weathered zones can be identified and their erosion resistance quantified, the identification of individual key rock blocks is not possible. Also rock geometry is simplified into 2D and although some account for the discontinuity structure with respect to the flow direction is given, the complete 3D nature of the joint orientations is not addressed.

The other prominent model for rock scour prediction is the Comprehensive Scour Model (CSM) by Bollaert (2002). Based on several near-prototype scale laboratory tests Bollaert examined the behavior of turbulent hydrodynamic pressures on plunge pool floors and in simplified rock joint geometries subject to an impinging water jet. The CSM is significant in that it attempts to represent the physics of the scour process and analyze the various scour mechanisms (brittle fracture, fatigue failure and block removal). The key components of Bollaert’s CSM are outlined in Figure 7.

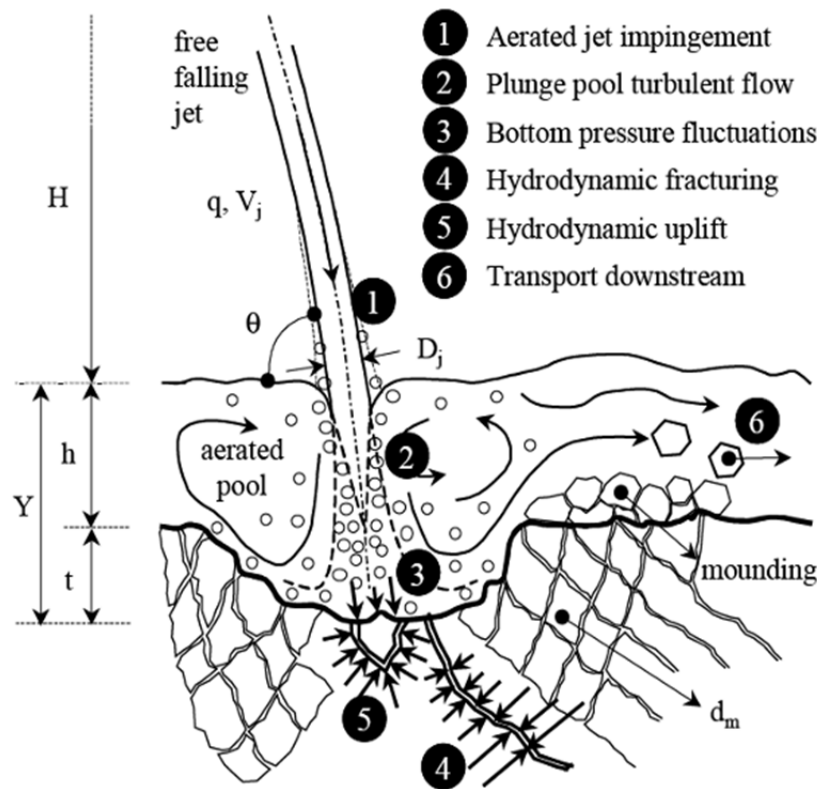


Figure 7: Key components of the CSM (Bollaert 2002).

Using fracture mechanics theory from Atkinson (1987) and testing results from Paris (1961) on metals, Bollaert (2002) developed relationships to evaluate the potential for intact rock to fail by brittle fracture or fatigue, respectively. He also examined the potential for lifting of individual block when subjected to dynamic pressure impulses from a jet impinging into a plunge pool. He found that transient pressures can develop beneath individual blocks via open joints surrounding the block, resulting in uplift (dynamic impulsion).

Block geometry, however, is simplified to rectangular blocks and no account is made for other joint orientations (Figure 8), such that lifting is the only mode of failure considered. Based on case study data, Bollaert & Schleiss (2005) calculated the block may be considered removed from the matrix when the uplift caused by a single pressure pulse ( $\Delta z$ ) is greater than about 20% of the vertical block dimension ( $z_b$ ) (i.e.,  $\Delta z/z_b > 0.20$ ).

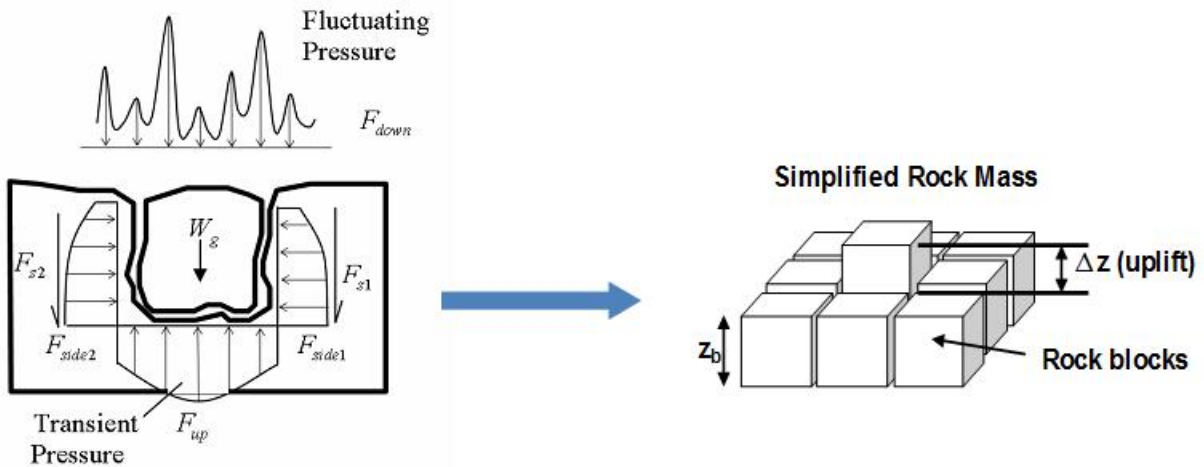


Figure 8: Bollaert block removal model.

Hydrodynamic pressures within the plunge pool are highly dependent on a number of factors including jet air entrainment, jet thickness, plunge pool depth, plunge pool geometry and air concentration in rock fissures and has been studied by many researchers (e.g., Ervine & Falvey 1987, Ervine et al. 1997, Castillo et al. 2007, Bollaert 2002, Manso 2006). The resulting dynamic pressure associated with the impinging jet can be quantified using the general equation below (from Bollaert 2002):

$$P = \gamma \cdot (C_p + \Gamma \cdot C'_p) \cdot \varphi \cdot \frac{v_j^2}{2g} \quad (3)$$

where  $\gamma$  = unit weight of water ( $N/m^3$ ),  $C_p$  = average dynamic pressure coefficient,  $C'_p$  = fluctuating dynamic pressure coefficient,  $\Gamma$  = amplification factor to account for resonance in close-ended rock

fissures (not applicable for block removal),  $\varphi$  = energy coefficient (usually assumed = 1),  $v_j$  = impact velocity of the jet (m/s), and  $g$  = acceleration of gravity ( $m/s^2$ ).

Evaluating the potential for intact rock fracture and block removal as a function of plunge pool depth provides the maximum scour depth achievable under a certain set of flow conditions as well as gives insight into the dominant scour mechanism occurring at various elevations in the plunge pool.

Federspiel et al. have extended the work of Bollaert to analyze the response of 3D cubic block due to vertical water jet impact in a plunge pool (previous measurements by Bollaert were for 2D block geometry). Early analysis of power spectral density curves indicated block response was solely limited to pressure fluctuations with low frequencies below approximately 10 Hz corresponding to larger-scale structures (eddies) within the plunge pool (2009) (Figure 9). More recent analysis has shown two additional peaks in the power spectral density curves at frequencies between approximately 20 Hz – 100 Hz and 100 Hz – 300 Hz, which the researchers suggest could be related to the fundamental resonant frequency of the pressure waves around the rock block or the eigen-frequencies of the block itself due to inertia (2011). In all scenarios, however, the amount of uplift of the block appears to be relatively small (approximately 1% of the vertical block dimension) and potentially shows the limitation of using a cubic block geometry where lifting is the only block failure mechanism.

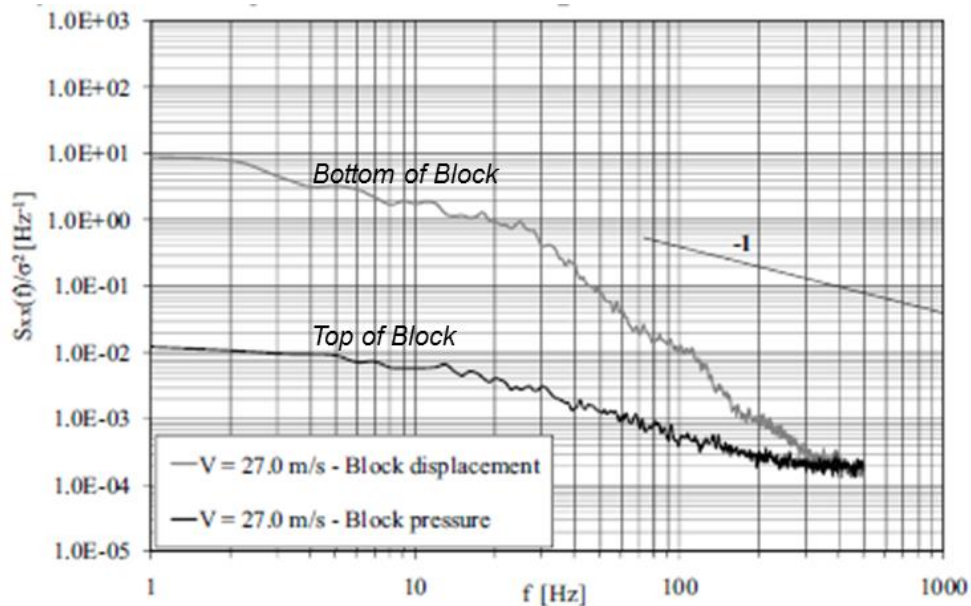


Figure 9: Non-dimensionalized power spectral density vs. frequency curve for pressure measurements at the top and bottom of a 3D cubic block. Note decline after approximately 10 Hz (Federspiel et al. 2009).

Asadollahi (2009) used the numerical Block Stability in 3D (BS3D) code (originally developed by Tonon 2007 and later modified by Asadollahi) to determine the dynamic uplift of the cubic block tested by Federspiel et al. (2009, 2011). BS3D considers all general failure modes of rock blocks subject to

generic forces. Using BS3D, Asadollahi found reasonable agreement between modeled and observed uplift when using actual pressure measurements around the block as input model parameters. Additionally, using data from Martins (1973) of physical model tests on cubic blocks in a riverbed and two case studies at the Picote Dam in Portugal and the Kondopoga Dam in Russia, Asadollahi used BS3D to slightly refine Bollaert's criteria, indicating a value of  $\Delta z/z_b > 0.25$  might be more representative of block removal.

George & Annandale (2006) modified Bollaert's CSM to evaluate the stability of abutment rock blocks subject to hydrodynamic forces from overtopping jet impact (Figure 10). Joint structure in 2D was analyzed and a relationship for the required rock bolt force to prevent dynamic impulsion was developed.

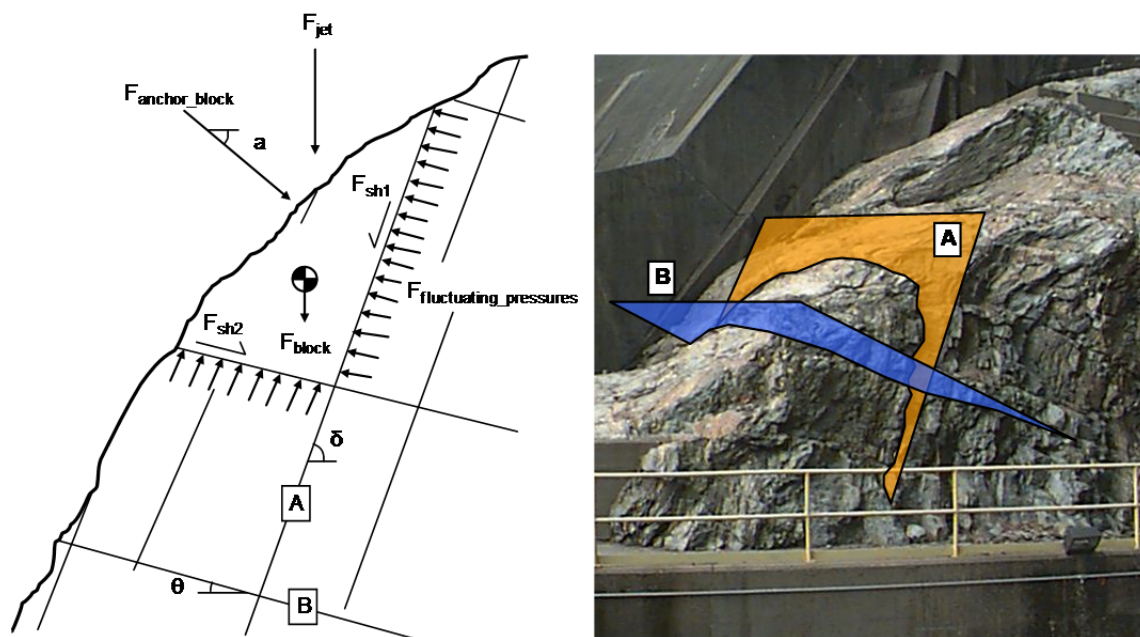


Figure 10: Analysis of abutment block due to overtopping jet impact (George & Annandale 2006)

Goodman and Hatzor (1991), in what may be the first 3D block scour analysis, performed an extensive examination of abutment stability using block theory for the Kendrick Dam Project in Wyoming. Large key blocks were identified based on joint orientations and a 3D block stability analysis was conducted. Only the static water pressure on the joint planes was considered for the overtopping jet and the role of the hydrodynamic pressures was unexamined. Similar analyses were presented by Goodman & Powell (2003) for other dam sites.

Reinus (1986) evaluated the removability of rectangular rock blocks subject to horizontal channel flows. He related the initial amount of protrusion of the block above the channel bottom to a critical flow velocity resulting in ejection. The United State Bureau of Reclamation (USBR) (2007) performed a

similar study looking at the hydraulic jacking of concrete slabs in lined spillway channels. They related the average stagnation pressure that develops underneath a slab (a function of the flow velocity) to the shape, offset and discontinuity aperture (gap) between two adjacent slabs (Figure 11).

Independently, both Bollaert (2010) extending the work of Reinus, and George (2010) using the work of the USBR, incorporated the influence of turbulent pressure fluctuations on the hydraulic jacking of rectangular blocks in channel bottoms. Based on research by Emmerling (1973) and Hinze (1975) (summarized in Annandale 2006), the magnitude of the pressure fluctuations,  $P'$  ( $N/m^2$ ), were quantified using:

$$P' = (3 \text{ to } 18) \cdot \tau_t \tag{4}$$

where  $\tau_t$  is the turbulent boundary layer shear stress ( $N/m^2$ ).

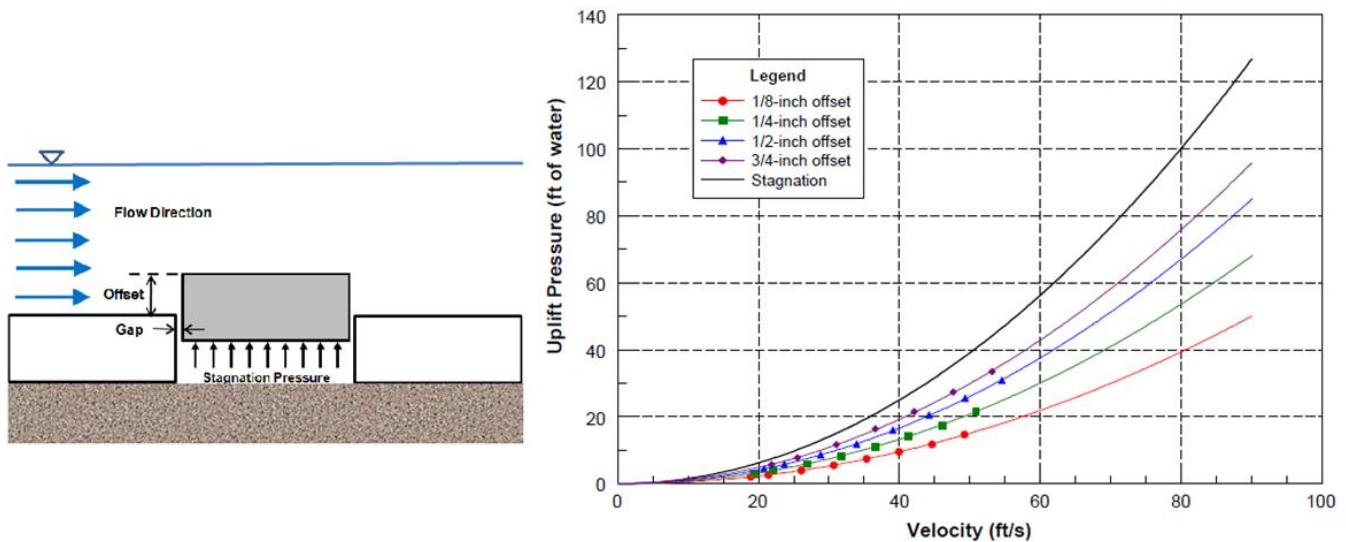


Figure 11: Hydraulic jacking of concrete spillway slabs (USBR, 2007)

Accordingly, the total lift applied to a protruding block is a function of the block buoyancy, quasi-steady (or pseudo-static) uplift resulting from build-up of stagnation pressure beneath the block, and the turbulent uplift resulting from pressure fluctuations (Figure 12) (Bollaert 2010). As implied, buoyancy and stagnation pressure are considered in a static manner, while the pressure fluctuations are analyzed in a dynamic sense. For a protruding block, and depending on the flow conditions, stagnation pressure or turbulent pressure fluctuations may be more dominant in causing uplift. However, for smaller block protrusions the stagnation pressure diminishes such that a block that is flush with the ground surface may only be removed by turbulent pressure fluctuations.

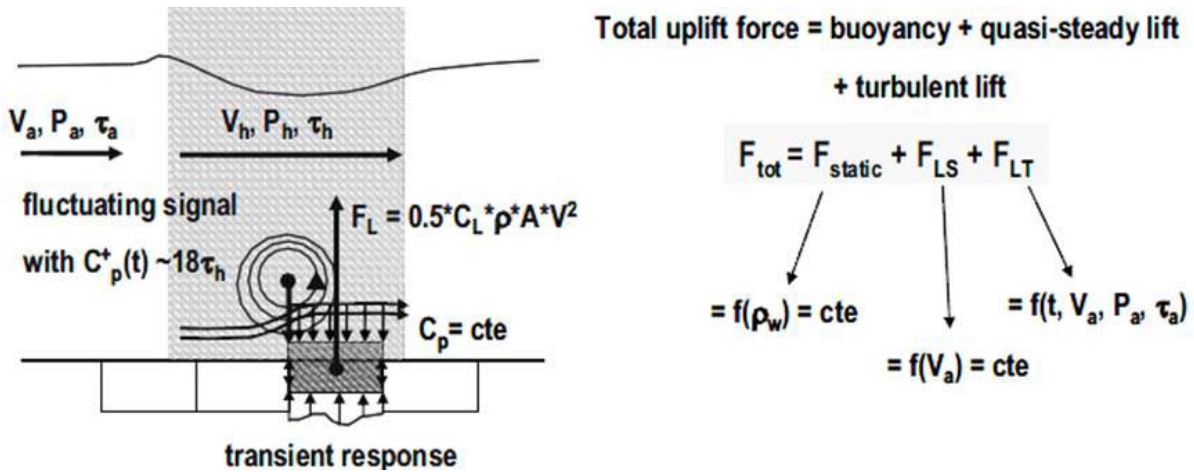


Figure 12: Block uplift at bridge pier (Bollaert 2010).

When considering turbulent uplift, Bollaert concluded that the critical flow velocity causing removal can be significantly decreased. For the flow scenarios analyzed by George, however, the influence of pressure fluctuations on uplift was found to be negligible. This suggests that some scenarios may be adequately analyzed in a pseudo-static manner, while for others a more dynamic representation is needed.

The majority of the above methods examine a single representative block subject to a characteristic hydraulic load dependent on the flow conditions and geometry. In the case of plunge pools, for example, if the representative block is removable at a certain elevation in the pool, scour will occur. The block is then analyzed again in a similar fashion at lower and lower elevations in the pool (corresponding to different hydraulic conditions) until the block is stable at which point scour is thought to cease. A few researchers, however, have begun analyzing multi-block systems through numerical analysis.

Multi-block analyses are significant in that the spatial estimates of scour may be obtained (opposed to simply determining scour initiation or maximum scour depth). Additionally, multiple block shapes and geometries may be considered. Wibowo (2009) applied key block theory from Goodman & Shi (1985) to find removable blocks exposed by an excavation for unlined rock spillways (Figure 13). Stability analyses were conducted for key blocks under flow conditions, however, it appears only 2D blocks were considered.

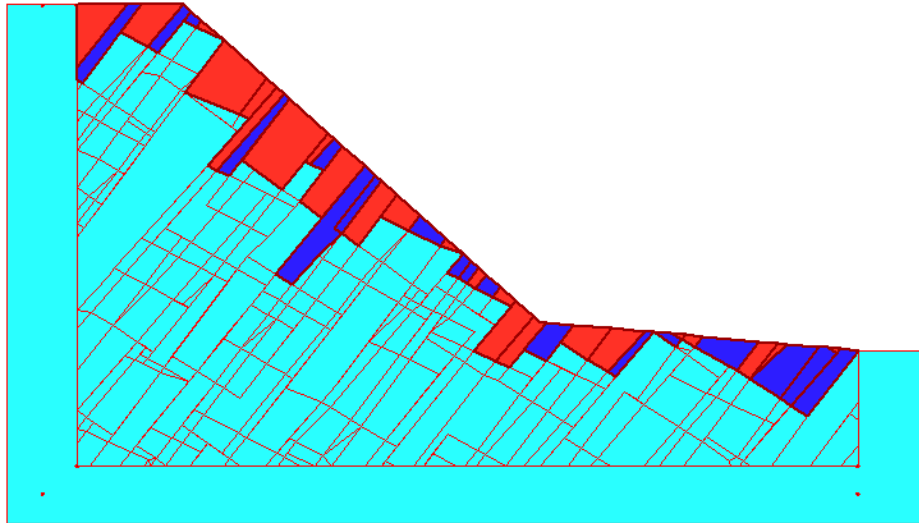


Figure 13: 2D removable blocks in unlined spillway (Wibowo 2009).

A similar attempt by Li and Liu (2010) was made, but for impinging jets into plunge pools. Removable 2D blocks were identified based on joint structure and corresponding plunge pool geometry was determined. Block stability was determined using empirical relationships for pressure distribution within the rock mass. Their simulated results yielded reasonable agreement with observed scour at the Xi Luo Du hydro-electric power plant in China.

More recently, Dasgupta et al. (2011) performed numerical simulations to estimate plunge pool scour formation at Kariba Dam in Zimbabwe. They used 3D computational fluid dynamics software (ANSYS FLUENT) to determine erosive capacities along with the 2D universal distinct element code (UDEC) to model the rock mass. Dynamic pressures at the bottom of the plunge pool were determined over a time interval and then input into UDEC to evaluate block removal and brittle fracture independently. Results from the block analysis and fracture analysis were superimposed to get an idea of the final scour hole shape, which showed reasonable agreement with that observed at Kariba Dam (Figure 14).

Interestingly, they found that blocks first to fail were just outside of the impingement region, which shows the importance of analyzing multiple block systems instead of a single representative block. Although the rock mass was modeled in 2D, their approach gives promise to the use of numerical methods to incorporate the 3D geometry of a rock mass along with complex flow conditions.

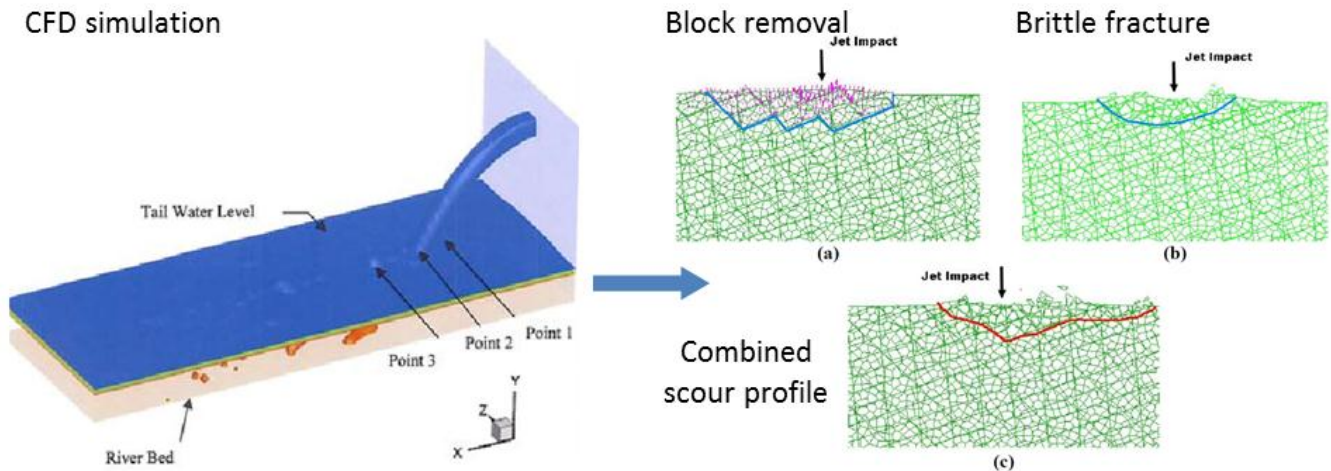


Figure 14: Numerical simulation of plunge pool scour (Dasgupta et al. 2011)

### 2.2.1 Limitations of Existing Scour Models

Empirical methods, such as Annandale's EIM, are limiting due to their inability to represent the physics of the scour process in that the mechanisms causing scour (block removal, fracture of intact rock) are not modeled. Additionally, these methods can be unreliable when used outside of their tested range.

Block models that incorporate simplified 2D rectangular or cubic block geometries, such as Bollaert's CSM, are limiting when orientations of the discontinuities are not orthogonal, such is commonly the case for igneous and metamorphic rock types. Furthermore, for such simplified geometries, block failure is limited to uplift and the potential for the kinematic sliding or rotation failure of rock blocks is not considered. 2D blocks that are not rectangular (such as those witnessed in the multi-block simulations above) are still restrictive in their ability to represent a rock mass and a process that is inherently 3D.

These limitations ultimately take away from the site-specific nature of the analysis being performed and accordingly may potentially yield unreliable results from which decisions concerning dam safety are made. An ideal scour model would represent an entire 3D rock mass comprised of multiple blocks while also evaluating 3D flow conditions that responded to changes in geometry due to scour progression over time. The effort required to develop such a model in any meaningful manner is great and demands complex numerical codes. As such, the focus of this research is to develop methodologies to analyze scour potential of single 3D rock blocks as well as to gain understanding that may be applied later to more complex 3D multi-block systems.

---

## 3. Methodology

To consider the 3D nature of rock blocks and their corresponding failure modes, block theory by Goodman & Shi (1985) has been applied. Block theory provides a rigorous methodology to identify removable blocks, determine potential failure modes, and assess block stability. Blocks that are most readily removable are termed key-blocks and are the locations where scour is likely to commence. Analysis may be performed graphically through stereographic projection or by vector solution, both of which are incorporated here. This section covers the basics of block theory analysis and its application to the scour problem.

### 3.1 Assumptions

The basic assumptions in block theory are: 1) all joint surfaces are planar, 2) joints extend completely through the volume of interest, and 3) blocks are assumed to be rigid. Some additional assumptions pertaining to assessment of scour for this paper are: 4) only tetrahedral blocks (defined by three joint planes and one free planar face) are considered; and 5) only the pure translation and pure rotation kinematic failure modes are considered. Initially these may appear to be limiting, however, a study performed by Hatzor (1992) examining block molds for a number of case histories indicated the majority of blocks removed were tetrahedral.

### 3.2 Removability

For a given set of three non-repeating joints (J1, J2, and J3) and one free face ( $f$ ), eight possible block shapes exist, one of which will be removable from the rock mass. Each block is termed a “joint pyramid (JP)” and is identified by a three number code relating to which side of the joint plane the block resides in space. A “0” indicates the block is above the joint plane while a “1” indicates the block is below the joint plane. For example, the JP code 001 indicates the block in question is above joint 1 (J1), above joint 2 (J2), and below joint 3 (J3). Using stereographic projection (Goodman 1976), the great circle corresponding to each joint set can be plotted thus subdividing the stereonet into regions corresponding to each JP (Figure 15). For an upper hemisphere stereonet, anything plotting inside the great circle for a particular joint is considered above that joint plane, while anything plotting outside is considered below.

To be removable, the JP region for a particular block must plot completely within the “space pyramid (SP)” as defined by the free face. The free face is essentially the rock/water or rock/air interface (assumed to be planar over the region of interest) that divides the SP (the region into which a removable block moves) from the “excavation pyramid (EP)” (the region where the block resides). For the example shown in Figure 15, JP 001 is a removable block from a horizontal free face, while JP 100 is a removable block from a vertical face striking East-West.

For rock masses with more than three joint sets, multiple combinations of three joint sets should be analyzed to find removable blocks in all cases. For example, if the total number of joint sets is four, the following sets should be analyzed with the free face: (J1, J2, J3), (J1, J2, J4), (J1, J3, J4) and (J2, J3, J4).

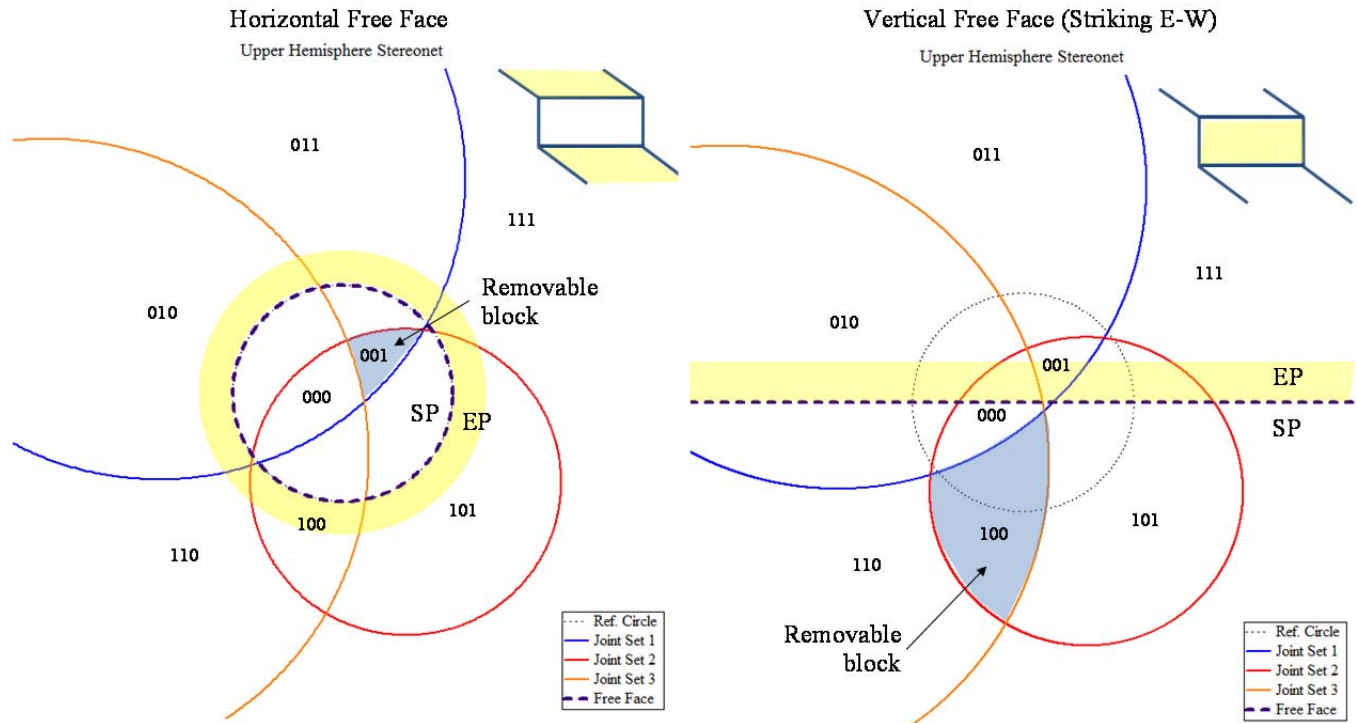


Figure 15: Upper hemisphere stereonet showing JP codes and removable blocks for horizontal free face (left) and vertical free face striking East-West (right).

### 3.3 Kinematic Mode Analysis

Once a block has been identified as removable, it is necessary to determine what kinematic modes of failure (Figure 5) are possible based on 1) block geometry and 2) orientation of the active resultant force being applied to the block. The active resultant is comprised of all the forces applied to the block which, for scour assessment, are namely the hydraulic forces and the self-weight of the block. For this section it is assumed the active resultant is arbitrary with some already known value. Suggestions for methods to determine the resultant for application of block theory to scour are discussed later on.

Criteria were developed by Goodman & Shi (1985) for assessing plausible kinematic failure modes for pure block translations and later by Mauldon & Goodman (1996) for pure block rotations. Criteria are provided below in vector form for simplicity, but may also be checked stereographically. Note **bold** font implies quantity is a vector.

For the pure translations, lifting of a block is kinematically feasible when:

---


$$\mathbf{s} \cdot \mathbf{v}_i > 0 \text{ for all } i \quad (5)$$

where  $\mathbf{s}$  = direction of block movement (equal to the direction of the active resultant,  $\mathbf{r}$ , for lifting), and  $\mathbf{v}_i$  = block-side normal vector for  $i^{\text{th}}$  joint plane. This condition indicates the direction of lifting is not parallel to any of the joint planes defining the block. The block-side normal may be calculated by:

$$\mathbf{n}_i = \begin{cases} \sin \alpha_i \cdot \sin \beta_i \\ \sin \alpha_i \cdot \cos \beta_i \\ \cos \alpha_i \end{cases} \quad (6)$$

$$\mathbf{v}_i = \mathbf{n}_i \text{ (block is above } i^{\text{th}} \text{ joint plane), } -\mathbf{n}_i \text{ (block is below } i^{\text{th}} \text{ joint plane)}$$

where  $\mathbf{n}_i$  = upward normal for the  $i^{\text{th}}$  joint plane and  $\alpha_i, \beta_i$  = the dip and dip direction, respectively, of the  $i^{\text{th}}$  joint plane. For block sliding on plane  $i$  only, the sliding direction is given by:

$$\mathbf{s} = \mathbf{s}_i = \frac{(\mathbf{n}_i \times \mathbf{r}) \times \mathbf{n}_i}{|\mathbf{n}_i \times \mathbf{r}|} \quad (7)$$

This is the orthographic projection of the active resultant onto the sliding plane. Kinematic feasibility of 1-plane sliding is subject to the following constraints:

$$\begin{aligned} \mathbf{v}_i \cdot \mathbf{r} &\leq 0, \text{ and} \\ \mathbf{s}_i \cdot \mathbf{v}_j &> 0 \text{ for all } j \neq i \end{aligned} \quad (8)$$

where  $j$  represents the remaining two joint planes. The first condition ensures a component of the resultant is projected onto the plane of sliding, while the second guarantees the block is being lifted from the remaining joint planes. For block sliding on planes  $i$  and  $j$  simultaneously, the sliding direction is given by:

$$\mathbf{s} = \mathbf{s}_{ij} = \frac{\mathbf{n}_i \times \mathbf{n}_j}{|\mathbf{n}_i \times \mathbf{n}_j|} \cdot \text{sign}[(\mathbf{n}_i \times \mathbf{n}_j) \cdot \mathbf{r}] \quad (9)$$

where  $\text{sign}(x)$  is a function that returns 1 if “ $x$ ” is positive and -1 if “ $x$ ” is negative. The sliding direction is along the line of intersection between the two planes. The  $\text{sign}$  function determines which direction sliding occurs along this line considering the orientation of active resultant. Kinematic feasibility of 2-plane sliding on planes  $i$  and  $j$  is subject to the following constraints:

$$\begin{aligned} \mathbf{s}_{ij} \cdot \mathbf{v}_k &> 0, \text{ and} \\ \mathbf{s}_i \cdot \mathbf{v}_j &\leq 0, \text{ and} \\ \mathbf{s}_j \cdot \mathbf{v}_i &\leq 0 \end{aligned} \quad (10)$$

where  $k$  represents the remaining joint plane from which the block is lifted.

For the pure translations, a block is kinematically rotatable about corner  $A_a$  for any applied resultant when (Tonon, 1997):

$$\begin{aligned}
 & \mathbf{v}_i \cdot \mathbf{v}_k \geq 0, \text{ or} \\
 & \mathbf{v}_j \cdot \mathbf{v}_k \geq 0, \text{ and} \\
 & (\mathbf{a}_G + \dot{\boldsymbol{\omega}} \times \mathbf{GA}_a) \cdot \mathbf{n}_i < 0, \text{ for } i = i \text{ and } j, \text{ and} \\
 & (\mathbf{a}_G + \dot{\boldsymbol{\omega}} \times \mathbf{GA}_b) \cdot \mathbf{n}_f < 0, \text{ for } b = b \text{ and } c
 \end{aligned} \tag{11}$$

where  $i$  and  $j$  are the joint planes containing the block corner in question (excluding the free face) while  $k$  corresponds to the remaining joint plane,  $\mathbf{a}_G$  = acceleration of the centroid ( $G$ ),  $\dot{\boldsymbol{\omega}}$  = angular acceleration about the rotation axis,  $\mathbf{GA}_a$  = vector from the centroid to the corner of rotation  $A_a$ , and  $\mathbf{GA}_b / \mathbf{GA}_c$  = the vectors from the centroid to the other corners ( $A_b$  and  $A_c$ ) on the block on the free face. The first two criteria are purely geometrical and ensure that at least one of the angles between either joint plane  $i$  or  $j$  and  $k$  is obtuse, thus allowing rotation. The remaining two ensure the corner of rotation moves against the block mold while the remaining two corners move into the space pyramid. The centroid acceleration may be calculated by:

$$\mathbf{a}_G = \frac{\mathbf{r}}{m} \tag{12}$$

where  $m$  = mass of the block. Additionally, the angular acceleration about the rotation axis is:

$$\dot{\boldsymbol{\omega}} = \frac{\mathbf{M}_G}{\mathbf{E}_G} \tag{13}$$

where  $\mathbf{M}_G$  = induced moment about the centroid and  $\mathbf{E}_G$  = inertial operator. See Tonon (1998) for additional details on determining  $\mathbf{E}_G$ . Note that the latter two conditions in (11) simplify to those provided by Mauldon & Goodman (1996) when no moment about the block centroid is considered (i.e.,  $\mathbf{M}_G = 0$ ). Finally, for the case of rotation about a block edge contained in the  $i^{\text{th}}$  joint plane with corners  $A_a$  and  $A_b$ , the following must be true:

$$\begin{aligned}
 & \mathbf{v}_i \cdot \mathbf{v}_j \geq 0 \text{ for all } j \neq i, \text{ and} \\
 & -\mathbf{v}_f \cdot \mathbf{v}_j \geq 0 \text{ for all } j \neq i, \text{ and} \\
 & (\mathbf{a}_G + \dot{\boldsymbol{\omega}} \times \mathbf{GA}_a) \cdot \mathbf{n}_i < 0, \text{ for } a = a \text{ and } b, \text{ and} \\
 & (\mathbf{a}_G + \dot{\boldsymbol{\omega}} \times \mathbf{GA}_c) \cdot \mathbf{n}_f < 0
 \end{aligned} \tag{14}$$

where  $f$  = the free face, and  $\mathbf{GA}_c$  = vector from the centroid to the remaining corner,  $A_c$ , on the free face. Since edge rotation is essentially an extension of corner rotation (i.e., rotation about two corners

simultaneously), the criteria above ensure both angles between the joint plane containing the free edge and the other two joint planes are obtuse as well as that block corner movements occur into the SP.

### 3.4 Stability

Once the feasible kinematic modes of block movement have been identified for removable blocks, block stability can be assessed. To assess stability, it is necessary to quantify the hydrodynamic forces applied to the block, their distribution on the block face and within the joints bounding the block. In doing so, it is important to consider the nature of the flow conditions, namely is flow turbulent with a large degree of variability causing significant pressure fluctuations such that a dynamic analysis is required or are the fluctuations small such that analyzing an average pressure in a pseudo-static sense may suffice. In either case, principles in block theory can be applied to give an estimate of block stability.

#### 3.4.1 Characteristic Hydrodynamic Pressure

For a given set of flow conditions, consider a corresponding characteristic dynamic pressure defined by an average dynamic pressure,  $P_m$  (or the dimensionless average dynamic pressure coefficient  $C_p$ ), a fluctuating dynamic pressure,  $P'$  (or the dimensionless fluctuating dynamic pressure coefficient  $C'_p$ ) and a frequency,  $\varepsilon$  (Figure 16).

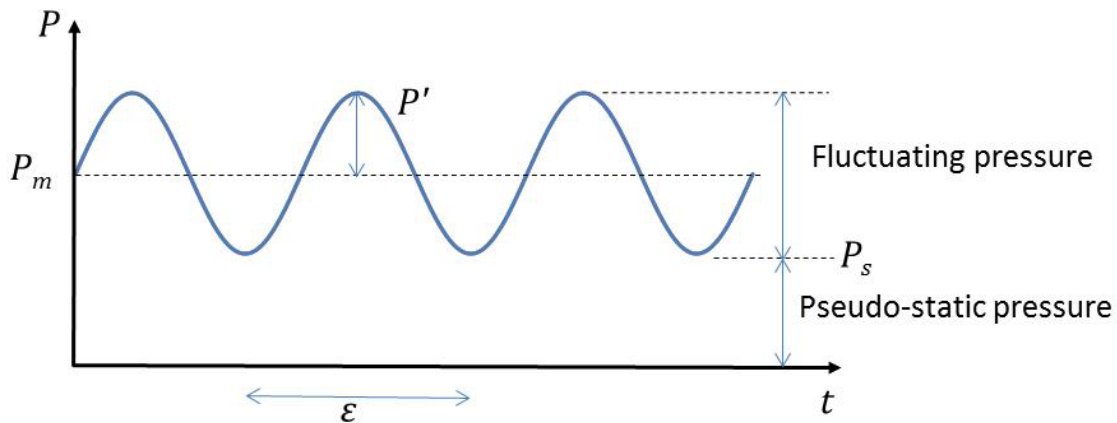


Figure 16: Characteristic dynamic pressure.

The characteristic dynamic pressure attempts to represent the main features of a flow field (as defined by the geometry, location, flow type, etc.) in a simplified manner. This characteristic pressure may be expressed as:

$$P = P' \cdot \sin(2\pi\varepsilon t) + P_m \quad (15)$$

As indicated in Figure 16 the characteristic dynamic pressure is comprised of two regions. The first is the fluctuating pressure region which represents the influence of the turbulent nature of the flow field. The second is the pseudo-static region where, for all practical purposes, the pressure is relatively constant and may be treated as such. When the pressure fluctuations are relatively small (i.e.,  $P' \ll P_m$ ), the pseudo-static pressure is approximately equal to the mean pressure and accordingly the flow may be analyzed in a pseudo-static manner (Figure 17 – top). Therefore the characteristic dynamic pressure can be approximated by the pseudo-static pressure,  $P_s$ .

$$P \cong P_s = P_m - P' \cong P_m \quad (16)$$

When the magnitude of the pressure fluctuations comprise a significant portion of the characteristic dynamic pressure (i.e.,  $P' \cong P_m$ ), the dynamic nature of the flow field cannot be neglected. For this analysis, the characteristic dynamic pressure will be converted to a single dynamic impulse which is then applied to a rock block to assess stability (Figure 17 – bottom). The reasoning for this is discussed in more detail later. The characteristic dynamic impulse can be expressed as:

$$P = P' \cdot \sin\left(2\pi\epsilon t + \frac{3}{2}\pi\right) + P_s \quad (17)$$

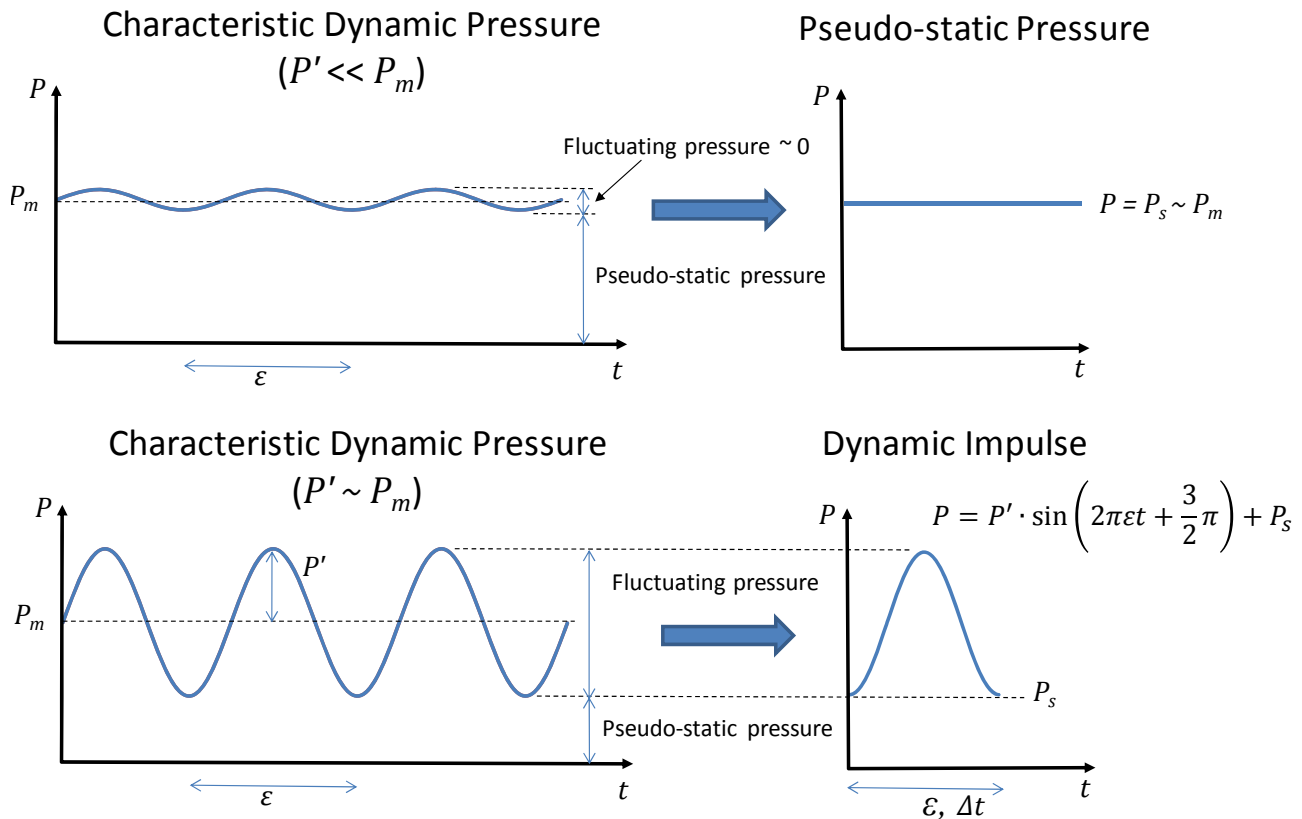


Figure 17: Simplification of characteristic dynamic pressure for pseudo-static (top) & dynamic (bottom) analyses.

---

### 3.4.2 Hydrodynamic Pressure Distribution on Block

Probably the biggest unknown for scour assessment of rock blocks is the hydrodynamic pressure distribution on the block faces. Little, if any, data exists regarding how hydrodynamic pressures change spatially and temporally around a 3D block, let alone a tetrahedral block. As such, assumptions must be made.

In situations where flow conditions are complex and turbulent (such as plunge pools, rough channel flows with complex geometries, hydraulic jumps, etc.) it is logical to think that dynamic pressures may be distributed around the block in many different combinations that continually change over time. Therefore, for dynamic analysis, hydrodynamic pressures are applied to all the different combinations of block faces assuming a uniform pressure distribution across the block face. For tetrahedral blocks there are 15 combinations of block faces (J1, J2, J3, or  $f$ ) to which pressure may be applied: J1, J2, J3,  $f$ , J1-J2, J1-J3, J1- $f$ , J2-J3, J2- $f$ , J3- $f$ , J1-J2-J3, J1-J2- $f$ , J1-J3- $f$ , J2-J3- $f$ , and J1-J2-J3- $f$ . These are referred to as “hydraulic load scenarios.”

This is a reasonable assumption as observations on the removal of rock blocks in laboratory studies by Yuditskii (1967) and later by Melo et al. (2006) have indicated that a single pressure fluctuation typically opens up one or two of the bounding joints (while subsequently closing the others) such that a large low frequency pressure fluctuation can cause significant pressure build-up in the open joints to eject the block. The assumption of uniform pressure distribution on block faces is likely valid only for blocks smaller than the characteristic length scale of large-scale eddies within the flow. For larger blocks, this may be too conservative. A similar approach is adopted by Asadollahi (2009) using BS3D code by Tonon (2007).

For pseudo-static analysis, a similar approach is adapted except that some of the hydraulic load scenarios may be excluded to account for a preferential flow direction (such as in a channel) where it may not make sense to have block movements upstream. This is discussed in more detail later on.

### 3.4.3 Pseudo-Static Block Stability

For scenarios when pressure fluctuations are small (i.e.,  $P' \ll P_m$ ) and the characteristic dynamic pressure may be approximated by a “constant” pressure, block stability may be evaluated in a pseudo-static manner using limit equilibrium analysis.

For each applicable hydraulic load scenario, the critical hydraulic force required to bring the block to limit equilibrium for each of the kinematically feasible block failure modes is determined. The equilibrium expressions are provided below (Goodman & Shi 1985):

$$F = |\mathbf{r}| \quad (\text{lifing}) \quad (18)$$

$$F = |\mathbf{n}_i \times \mathbf{r}| - |\mathbf{n}_i \cdot \mathbf{r}| \cdot \tan \varphi_i, \text{ for all } i \quad (1 - \text{plane sliding}) \quad (19)$$

---


$$F = \frac{1}{|\mathbf{n}_i \times \mathbf{n}_j|^2} \cdot [|\mathbf{r} \cdot (\mathbf{n}_i \times \mathbf{n}_j)| \cdot |\mathbf{n}_i \times \mathbf{n}_j| - |(\mathbf{r} \times \mathbf{n}_j) \cdot (\mathbf{n}_i \times \mathbf{n}_j)| \cdot \tan \varphi_i - |(\mathbf{r} \times \mathbf{n}_i) \cdot (\mathbf{n}_i \times \mathbf{n}_j)| \cdot \tan \varphi_j]$$

*for all  $i \neq j$ , (2 - plane sliding)*

(20)

where  $F$  = fictitious, required stabilizing force applied in the direction of movement to maintain equilibrium (N),  $\varphi_i$  and  $\varphi_j$  = friction angles (deg) on joints  $i$  and  $j$ , respectively, and  $\mathbf{r}$  = active resultant force (N). When  $F$  is negative the block is considered stable, and when  $F$  is positive the block is unstable. When  $F$  is zero, the block is in equilibrium such that any further increase in the pressure will result in removal of the block.

The resultant,  $\mathbf{r}$ , can be calculated as follows:

$$\mathbf{r} = \sum_{i=1}^x (P \cdot A'_i \cdot \mathbf{v}_i) + m \cdot \mathbf{g}$$
(21)

where  $P$  = pseudo-static pressure which is varied until limit equilibrium is reach (N/m<sup>2</sup>),  $A'_i$  = area of  $i^{th}$  joint plane (m<sup>2</sup>),  $\mathbf{g}$  = acceleration due to gravity (m/s<sup>2</sup>), and  $x$  = number of block faces being analyzed.

As it is assumed that any of the pressure combinations being analyzed are plausible, the one yielding the lowest hydraulic force to result in block failure is considered to be the most critical.

Note that only expressions for the translations are provided. Because the orientation of the active resultant is assumed to potentially vary in all directions, the most critical mode will almost always be one of the translations unless the friction angle of the rock joint is very high. Furthermore, the probability that a block is removable and rotatable is fairly low (~16%) (Mauldon 1990). As such, only 1-plane sliding, 2-plane sliding and lifting need be considered here.

To illustrate this procedure, consider a removable tetrahedral block bounded by joints J1, J2, J3 and a free face,  $f$ , with known surface areas. For the case that pseudo-static pressure is only applied to J3, for example, using the criteria in Equations (5), (8) and (10) the only kinematically feasible mode is 2-plane sliding (i.e., sliding on J1 and J2). Subsequently, using Equation (19) the value of  $F$  is plotted as a function of the pseudo-static pressure head (Figure 18). As indicated,  $F$  is negative for all values of pressure head indicating the block will remain stable under this hydraulic load configuration. For the case when pressure is applied to block faces J2 and J3,  $F$  is negative initially, but at a pressure head of approximately 0.6 m,  $F$  becomes positive indicating the block will fail by sliding on J1.

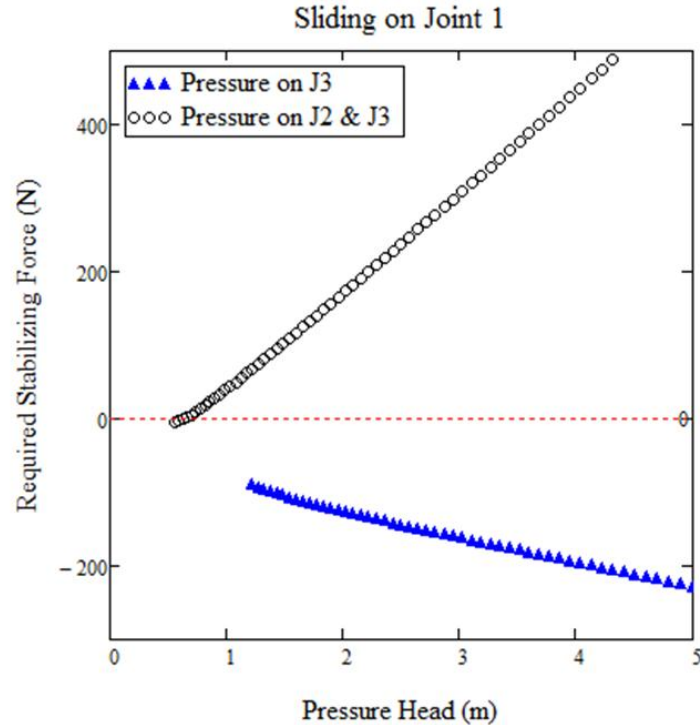


Figure 18: Example of vector solution for a removable block with hydraulic load applied to block face J3 and when applied to faces J2-J3.

This procedure can also be shown graphically on the stereonet. Figure 19 presents a limit equilibrium net for the same removable block used in the example above, constructed using methodologies from Goodman & Shi (1985). The stereonet is divided into regions that represent all the potential modes of translational failure for a given removable block. The region in which the active resultant plots corresponds to the mode of translation that will occur provided joint friction (represented by the colored contours) is not adequate to keep the block in place. For this particular plot, a friction angle of 40 degrees (solid red contour line) has been chosen to represent the strength of the rock joints. This contour represents a state of limit equilibrium for the block (corresponding to  $F = 0$  in the vector solution). Should the active resultant plot outside of this region, movement in the corresponding mode will occur.

Also shown in Figure 19 is the active resultant path for the hydraulic load scenario when pseudo-static pressure is applied to block face J3 and for the case when pressure is applied to J2 and J3. For both cases, the resultant path begins at the center of the stereonet as initially the only force applied to the block is its weight which acts straight down. As pressure on J3 increases, the resultant orientation changes, but never crosses the contour corresponding to a joint friction angle of 40 deg., indicating the block is always stable. This is because the block-side normal vector for J3 plots inside of the limit equilibrium contour. This is not the case when pressure is applied on J2 and J3. Increasing pressure on

J2 and J3 results in the active resultant path crossing the limit equilibrium contour indicating the block will become unstable and sliding on J1 will occur.

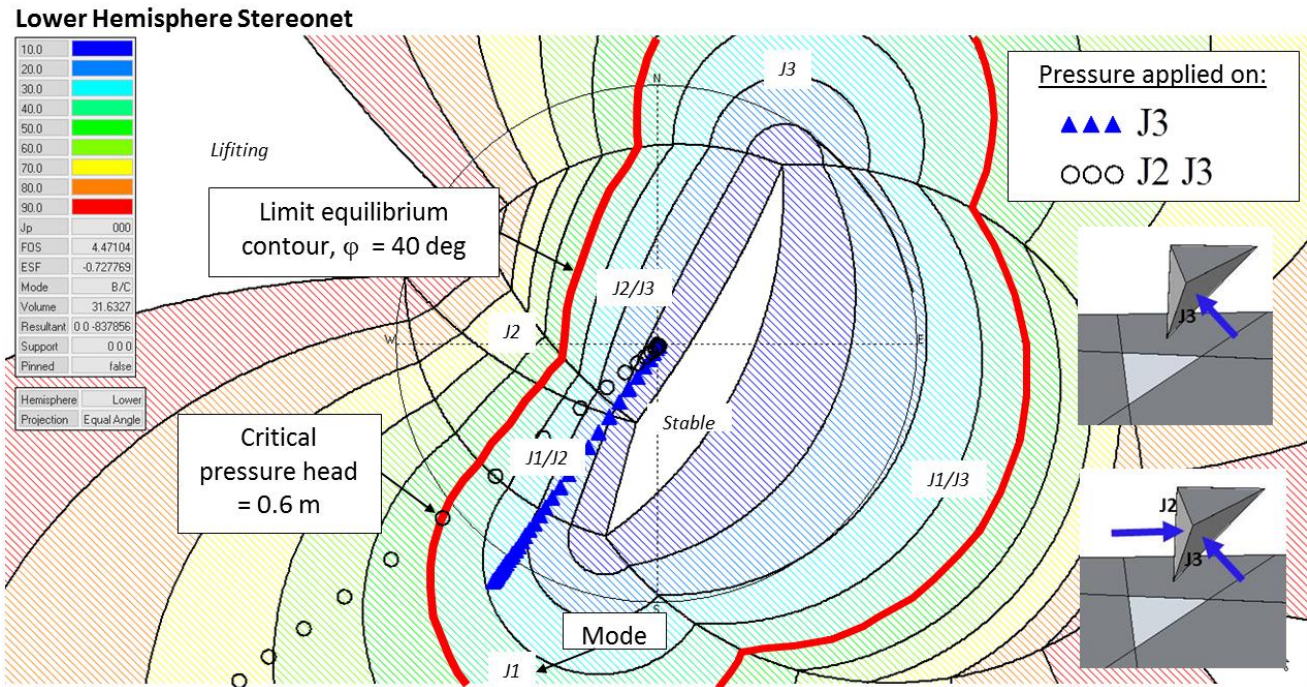


Figure 19: Example of limit equilibrium stereonet for removable block showing resultant paths for hydraulic load applied to block face J3 and J2-J3 (stereonet generated with PanTechnica (2002) software).

### 3.4.4 Dynamic Block Stability

When the magnitude of the pressure fluctuations comprise a significant portion of the characteristic dynamic pressure (i.e.,  $P' \cong P_m$ ), the dynamic nature of the flow field cannot be neglected. For this analysis, the characteristic dynamic pressure is converted to a single dynamic impulse which is then applied to a rock block to assess stability (Figure 17 – bottom).

As described above, observations by Yuditskii (1967) and later by Melo et al. (2006) have indicated that a single pressure fluctuation typically opens up one or two of the bounding joints (while subsequently closing the others) such that a large low frequency pressure fluctuation can cause significant pressure build-up in the open joints to eject the block. As such, it seems appropriate for dynamic analysis to consider the response of a rock block to a single characteristic dynamic impulse.

For dynamic flow conditions, it is hypothesized that the resultant hydraulic force will change in magnitude and orientation over time. As such, it is assumed that all 15 hydraulic load scenarios are plausible for a tetrahedral block. The removal of a rock block, therefore, will likely occur in a mode that requires the least applied hydraulic force.

For simplicity, pseudo-static analysis of the removable block in question can first be performed to determine which mode is most critical (as described above). Once the critical mode has been determined, the block may be analyzed in a more dynamic sense by determining the displacement of a block in the modal direction subject to a single characteristic pressure fluctuation (dynamic impulse). For all practical purposes the shape of the force over time can be assumed sinusoidal, while the duration is related to the frequency, which for block removal is on the order of magnitude around 1Hz (Firoto & Rinaldo 1992, Federspiel et al. 2009).

The impulse,  $I$  (N·s), can be calculated by:

$$I = \int_0^{\Delta t} F_c(t) dt = mV_{\Delta t} - 0 \quad (22)$$

Where  $F_c(t)$  = expression for the fictitious required stabilizing force (now a function of time) related to the critical mode determined above,  $V_{\Delta t}$  = block velocity in the direction of movement after the duration of the pulse (assuming the initial velocity is zero) (m/s). Note that integration should only occur for positive values of  $F_c(t)$  (i.e., when the hydraulic forces exceed the resistance of the block indicating displacement is occurring). Therefore the integration limits ( $\Delta t$ ) shall be narrower than the duration of the characteristic pressure fluctuation. Making use of Equation (17), the active resultant for calculation of  $F_c(t)$  is:

$$\mathbf{r}(t) = \sum_{i=1}^x \left( \left( P' \cdot \sin \left( 2\pi\epsilon t + \frac{3\pi}{2} \right) + P_s \right) \cdot A'_i \cdot \mathbf{v}_i \right) + m \cdot \mathbf{g} \quad (23)$$

Again,  $x$  = number of block faces being analyzed corresponding to the critical hydraulic load scenario.

At the end of the impulse, the block is left with some initial velocity from which a displacement can be calculated. The time to bring the block to rest, either by friction (for sliding) or by gravity (for lifting) can be calculated as:

$$\Delta t^* = \frac{0 - mV_{\Delta t}}{F_c^*} \quad (24)$$

where  $F_c^*$  = expression for the fictitious stabilizing force related to the critical mode determined above (N), with the active resultant force,  $\mathbf{r}$ , now being solely a function of the weight of the block (i.e., no hydrodynamic pressure). For block sliding, either 1-plane or 2-plane, the joint friction angles in (19) and (20) should reflect a mobilized strength as the block is now in motion. For block uplift, since the

---

only resistance is gravity, it is necessary to calculate the component of the velocity in the vertical ( $z$ ) direction in order to properly determine the time for the block to reach its peak height. This can be done simply by:

$$V_{\Delta t_z} = V_{\Delta t} \cdot \left( \frac{\mathbf{r}(\Delta t)}{|\mathbf{r}(\Delta t)|} \cdot (0 \ 0 \ 1) \right) \quad (\text{for lifting only}) \quad (25)$$

The subsequent displacement,  $\Delta l$  (m), associated with the impulse is then:

$$\Delta l = V_{\Delta t} \cdot \Delta t^* + \frac{1}{2} \left( \frac{F_c^*}{m} \right) \cdot (\Delta t^*)^2 \quad (26)$$

To assess if a block remains in its mold, a criteria relating displacement to block removal is needed. As mentioned above, Bollaert (2002) related the ratio of the amount of uplift for a rectangular block (due to a single impulse) to the vertical block dimension and found that for a ratio of approximately 0.20 or greater, the block could be considered removed. Asadollahi (2009) refined this estimate for rectangular blocks using the BS3D code and found a ratio of 0.25 may be more adequate based on additional case study data. If a similar approach is adopted for tetrahedral blocks a characteristic length scale is needed to compare with the amount of displacement. At this time no criteria for removal is proposed but it is hypothesized when considering other modes of block failure (by considering 3D block geometry) this ratio may be significantly smaller for some blocks and higher for others.

---

## 4. Results (Case Study)

The above methodology has been used to assess scour potential of an actively eroding unlined rock spillway channel at a dam site in northern California. For this case study, field investigations were performed to collect pertinent rock mass information and analyses were conducted to identify removal blocks and determine their susceptibility to scour.

### 4.1 Project Background

The dam site is located in the Sierra Mountains of northern California along Interstate 80 near Donner Pass. The dam, originally constructed in 1919, has both a primary and secondary (emergency) spillway located on the northern side of the reservoir. The primary spillway consists of ten radial spillway gates that discharge directly into a rock lined valley comprised of jointed granodiorite (Figure 20). Snowmelt from the Sierra fills the reservoir in the Spring typically resulting in continued discharge from approximately April to July. The design capacity of the primary spillway is approximately 55,000 ft<sup>3</sup>/s with an additional capacity of 7,500 ft<sup>3</sup>/s provided by the emergency spillway. The flood of record occurred in 1997 with a discharge of approximately 20,000 ft<sup>3</sup>/s. Based on communication with site personnel the actual discharge was likely larger (~25,000 ft<sup>3</sup>/s) due to failure of the stream gauges downstream during the rising portion of the flood hydrograph.

Since operation, however, significant erosion of the unlined spillway has occurred at discharges much less than the flood of record resulting in the formation of an actively retreating slot canyon (Figure 20). Based on measurements made of the alluvial fan at the mouth of the spillway canyon using aerial photography, it is estimated approximately 6,500,000 ft<sup>3</sup> of intact rock material has been scoured away (Figure 21).

Remedial measures such as rock bolting and installation of a concrete apron near the spillway gates, based on recommendations from previous investigators (e.g., Goodman & Powell 2003), appear to have temporarily retarded scour migration.



Figure 20: Canyon formed by scour showing spillway gates in background (left). Approximately 2,000 cfs discharge in June 2010 (right).



Figure 21: Aerial view of spillway showing alluvial fan of eroded material (note the walkway across the primary spillway is approximately 300 ft long for scale).

---

## 4.2 Field Investigations

Field investigations were carried out to determine pertinent rock mass parameters (namely joint orientations and spacing). To do this, scan-line surveys were performed within the spillway area using a tape measure and Brunton geologic compass. Additional joint orientations were obtained by measuring discontinuities bounding block molds (i.e., locations where blocks had previously been removed). Scan-line and block mold locations are shown in Figure 22.



Figure 22: Scan-line survey and block mold locations (left), NE striking scan-line survey (upper right), block mold below spillway gate (lower right).

Aerial Light Detection and Ranging (LiDAR) was also provided by the dam owner. Spatial values from the LiDAR data set were extracted and input into Meshlab (2011), an open source software for processing and editing 3D triangular meshes. Normal vectors to the mesh, relating to the normal orientations of the joint faces on rock mass could be output such that the orientations of the joint sets could be obtained (Figure 23).

Due to the presence of numerous steeply dipping joint sets at the spillway site that could not be adequately capture by aerial LiDAR measurements, the data were biased toward the more horizontally dipping joints. Because of this bias, priority was given to orientations obtained from hand measurements.

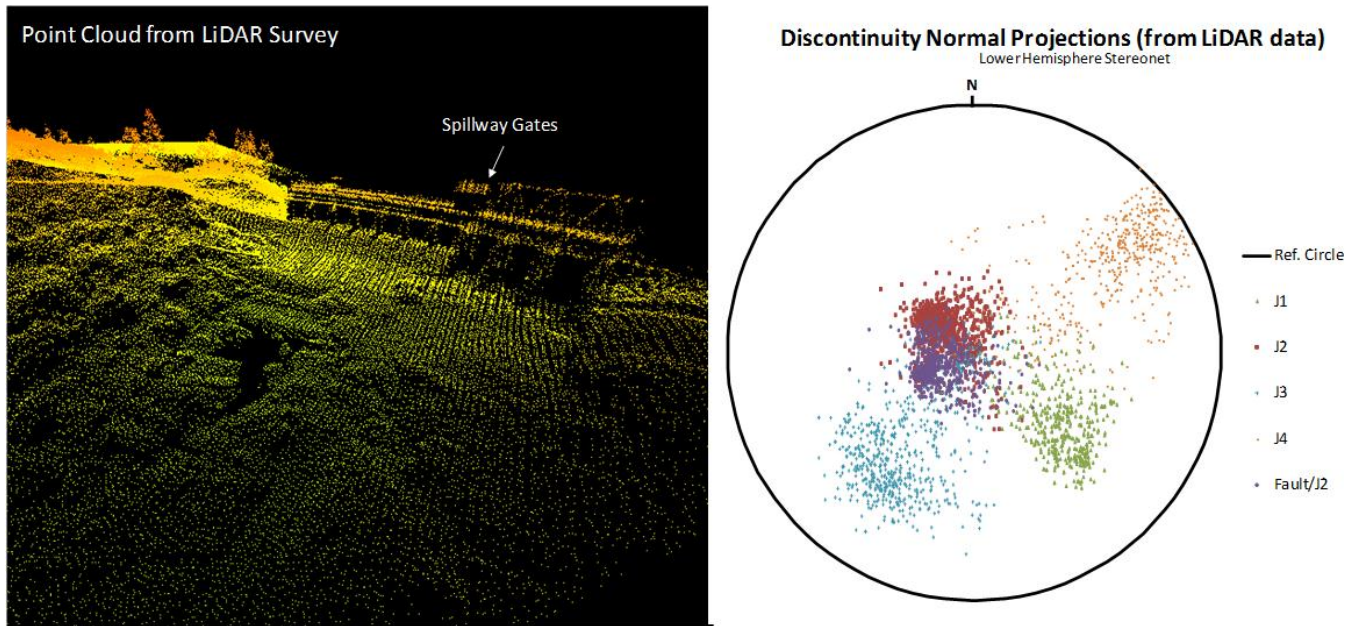


Figure 23: Aerial LiDAR point cloud of primary spillway (left), and stereographic projection of joint normal orientations from LiDAR data (right).

Joint data used for subsequent block theory analysis are summarized in Table 1 and shown graphically on the stereonet in Figure 24. In all five joint sets were identified, with average spacings ranging between approximately 0.5 m to 1.3 m.

Table 1: Summary of joint data used for block theory analysis.

Joint Set	Orientation (deg)			Avg. Spacing (m)
	Strike	Dip Direction	Dip	
1	230	320	69	1.04
2	55	145	45	0.49
3	309	39	82	1.04
4	132	222	83	1.31
5	168	258	70	0.46

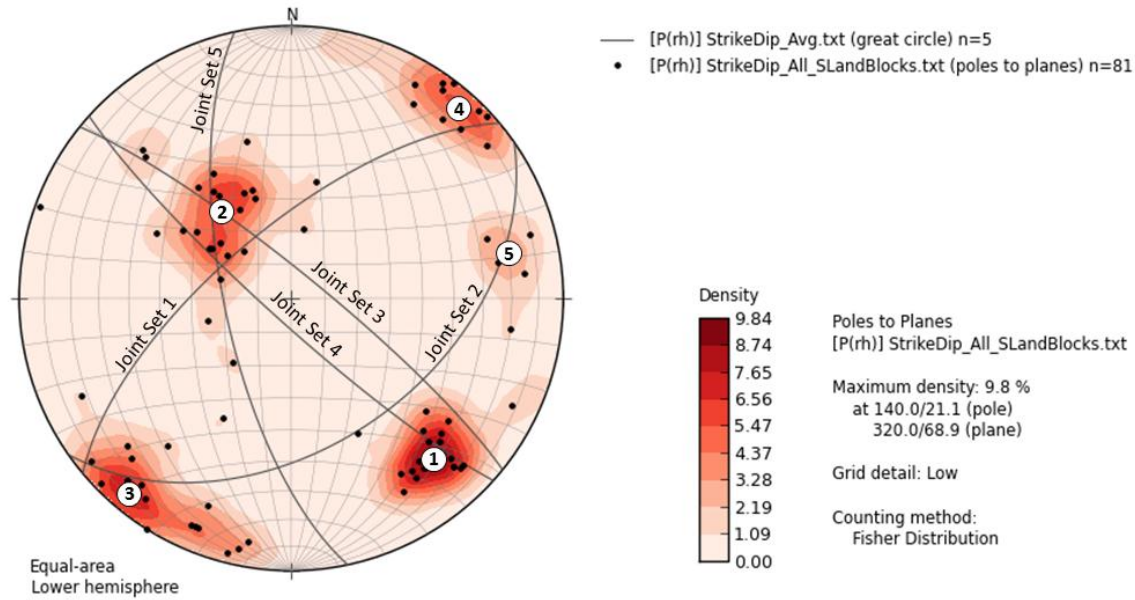


Figure 24: Stereographic projection of hand-measured joint data (plotted in OpenStereo (Grohmann and Campanha 2011)).

### 4.3 Scour Assessment using Block Theory

For simplicity here, erodibility assessment of the spillway has been limited to a single free rock face, although a more thorough analysis would consider all pertinent locations / faces. The free face in question is that directly downstream of the spillway gates. Based on field measurement, the spillway face has an orientation of 320 / 10 (dip direction / dip) in degrees. A schematic of the simplified scenario being analyzed is shown in Figure 25.

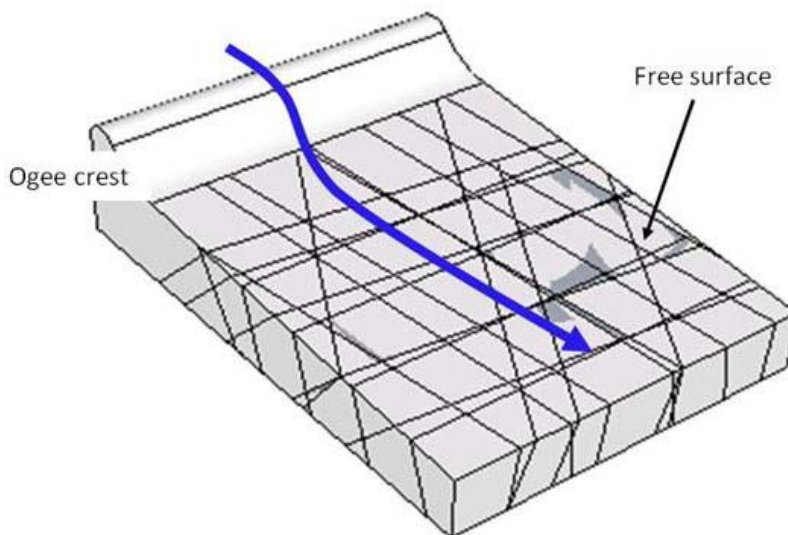


Figure 25: Simplified spillway schematic.

### 4.3.1 Removability

Since only tetrahedral blocks are considered, the five joint sets above were broken down into groups of three that, when combined with the free spillway face, will yield a four-sided (tetrahedral) block with no repeated joint sets. In doing so, there are ten different combinations (joint groups) that require analysis, each of which will produce one removable block. Using stereographic projection, the removable JP code was determined (Figure 26). The JP codes are identified by joint group in Table 2 with the stability results.

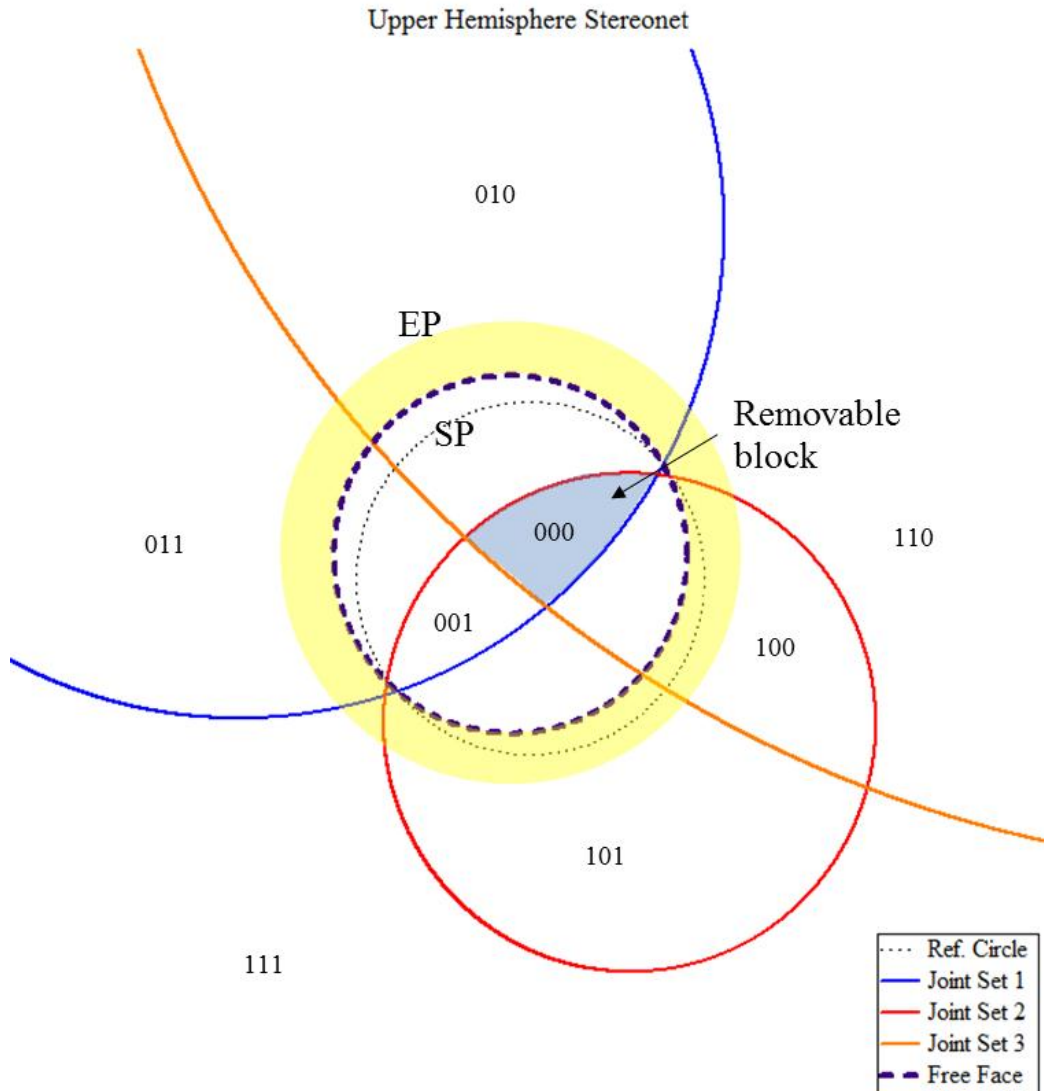


Figure 26: Stereonet showing removable block for joint group containing J1, J2, J3, and *f*.

### 4.3.2 Stability

Once all the removable blocks were identified, their stability could be assessed. The hydraulic load applied to the blocks was determined using research by the USBR on hydraulic jacking of concrete slabs

(2007, Figure 11). Due to the relatively rough nature of the spillway channel, it was assumed removable blocks had a slight protrusion above the channel such that stagnation pressure from flow impact would develop around the block. At this time, only pseudo-static analysis was performed and the additional influence of dynamic impulses was not considered.

Because flow in the spillway channel is predominantly unidirectional, particularly right below the spillway gates, it was decided to limit the orientation of the active result paths to an approximately 60 degree window shown in the Northwest quadrant of the stereonet (Figure 27). This is a reasonable assumption as a block moving against the direction of flow seems unlikely unless very large pressure fluctuations are present. This greatly reduced the number of stability analyses to be performed from 150 (15 hydraulic load scenarios for 10 removable blocks) to 35. Note, the angle for the window was arbitrarily selected and may be a topic for further research.

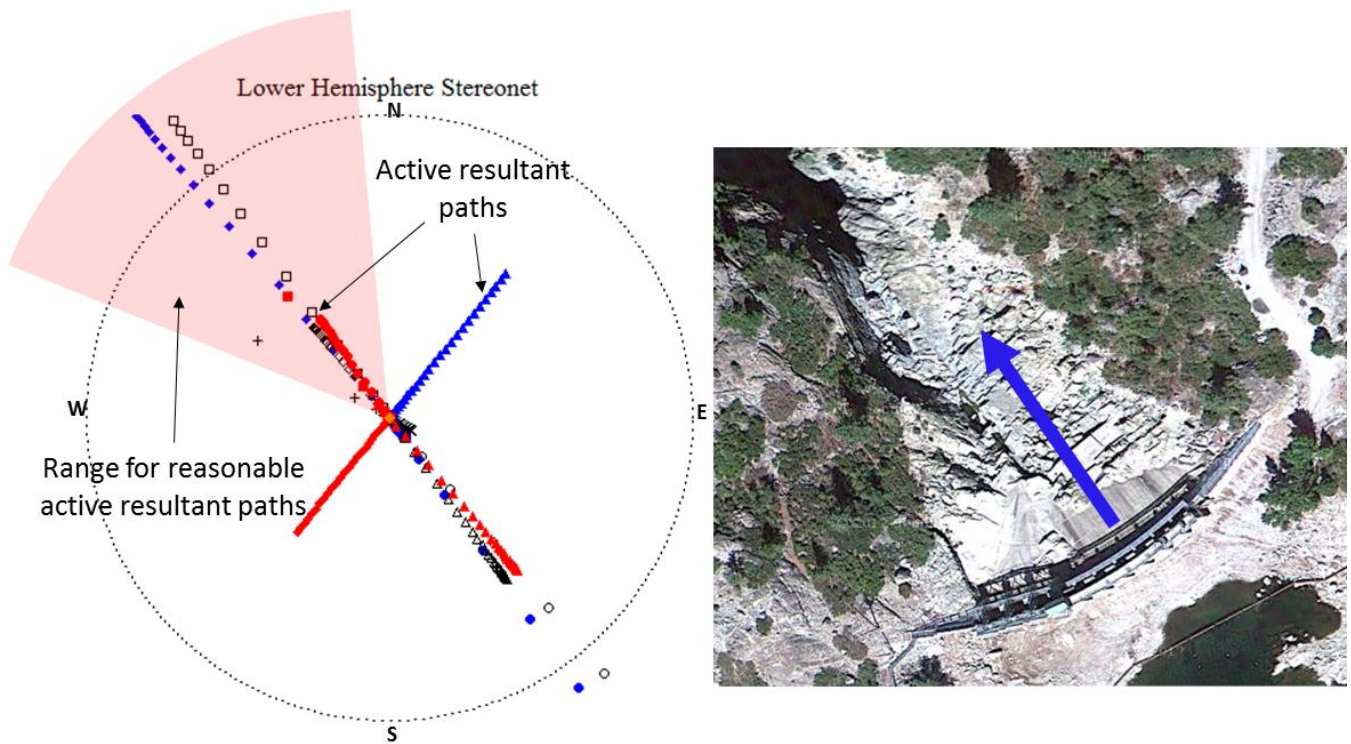


Figure 27: Limitation of active resultant paths for removable blocks (left) due to dominant flow direction in the spillway channel (right).

Block stability was assessed in vector format using Equations (18), (19) and (20) subject to the criteria in Equations (5), (8) and (10). The fictitious required stabilizing force,  $F$ , was plotted as a function of the flow velocity to determine the critical velocity resulting in removal of the block.

Figure 28 shows block stability for the most critical removable block originating from the joint group containing J1, J2, and J5. As indicated, at a flow velocity of 4.4 m/s the block will fail by 2-plane sliding

(on J2 and J5) for a hydraulic pressure that is distributed uniformly across J1, J2, and J5. At a slightly higher flow velocity, a pressure distribution on J1 and J2 will also cause 2-plane sliding on J2 and J5. It is interesting to follow the active resultant path for these two hydraulic load scenarios as the velocity is increased. At approximately 4.9 m/s, 2-plane sliding is no longer kinematically feasible and in both scenarios, the mode changes to 1-plane sliding on J5. For the scenario when pressure is applied to J1 and J5, the 2-plane sliding on J2 and J5 is feasible at low velocities but does not become critical until flow velocity is approximately 20 m/s (not shown on the plot). Finally, if pressure is applied to J1, 2-plane sliding on J2 and J5 is also feasible at low velocities, however, increased flow velocity only provides more stability to the block.

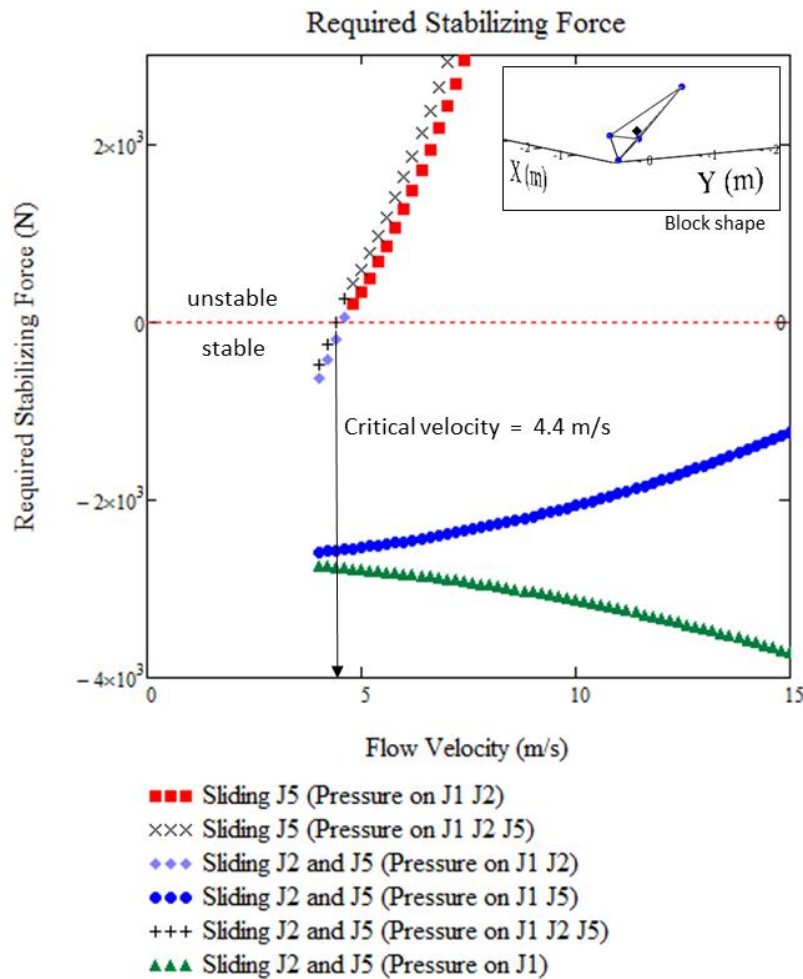


Figure 28: Stability of most critical removable block from spillway channel.

The stability results for all the removable blocks are listed in Table 2. Provided are the corresponding JP codes, the applicable hydraulic load scenarios (i.e., the load scenarios yielding an active resultant path that fits within the window shown in Figure 27), the kinematically feasible failure mode for each hydraulic load, the critical load scenario, the critical failure mode and finally the critical flow velocity.

Table 2: Block stability results summary.

Joint Group	JP Code	Applicable Hydraulic Load Scenarios	Failure Mode	Critical Load Scenario	Critical Mode	Critical Velocity (m/s)
J1 J2 J3 f	000	J1	S2	J1 J2 J3	L	4.7
		J1 J2	L			
		J1 J3	S2			
		J1 f	-			
		J1 J2 J3	L			
		J1 J3 f	-			
J1 J2 J4 f	001	J1	S24	J1 J2 J4 & J1 J2	S4	4.6
		J2	S4			
		J1 J4	S2			
		J1 f	-			
		J1 J2 J4	S4			
		J1 J4 f	-			
J1 J2 J5 f	001	J1	S25	J1 J2 J5	S25	4.4
		J1 J2	S25, S5			
		J1 J5	S25			
		J1 f	-			
		J1 J2 J5	S25, S5			
		J1 J5 F	-			
J1 J3 J4 f	100	J3 J4	-	-	-	-
		J1 J3 J4	-	-	-	-
J1 J3 J5 f	100	J3 J5	S1	J1 J3 J5	S1	8.0
		J1 J3 J5	S1			
		J3 J5 f	-			
J1 J4 J5 f	110	J4 J5	-	-	-	-
		J4 J5 f	-	-	-	-
J2 J3 J4 f	000	J3 J4	S2	J2 J3 J4	S2	11.9
		J2 J3 J4	S2			
J2 J3 J5 f	000	J3 J5	S2	J2 J3 J5	S2	5.0
		J2 J3 J5	L, S2			
		J3 J5 f	-			
J2 J4 J5 f	010	J4 J5	S24,S2	J2 J4 J5	S24	4.4
		J2 J4 J5	S24, S2, L, S4			
		J4 J5 f	-			
J3 J4 J5	001	J3 J4	-	-	-	-
		J3 J4 J5	-	-	-	-

**Notes:**

L – lifting

SX – 1-plane sliding on Joint X

SXY – 2-plane sliding on Joint X and Joint Y

---

As indicated in Table 2, critical velocities resulting in block removal range from 4.4 m/s to 11.9 m/s. It should be noted that a few joint groups did not yield any block that could kinematically be removed.

Additional result plots and calculations are provided in Appendix A.

---

## 5. Conclusions

Scour of rock is a complex process where the removal of individual rock blocks is one of the principal mechanisms by which scour can occur. Until now, the geologic structure of the rock mass (which strongly influences block removal) has been treated in a simplified manner such that the ability to perform a site-specific analysis has been limited.

In this research, a framework has been developed in which block theory can be applied to evaluate the scour potential of 3D rock blocks. The main considerations for using block theory to evaluate erodibility are:

1. rock mass geometry (namely discontinuity orientations and spacing to determine block shape, size and removability),
2. flow conditions (pseudo-static or dynamic),
3. hydrodynamic pressure distribution on rock block, and
4. block stability

### 5.1 Rock Mass Geometry

Rock mass data are determined through field investigations. For this analysis, scan-line survey data and aerial LiDAR data were used to determine discontinuity orientations and spacing. Preference was given to hand measurements, as the LiDAR data showed a bias to more horizontally dipping joint sets. In all, five joint sets were measured (Table 1). Since only tetrahedral blocks are considered, the five joint sets were broken down into groups of three that, when combined with the free spillway face, yield a four-sided (tetrahedral) block with no repeated joint sets. In doing so, ten different combinations (joint groups) were analyzed, each of which produced one removable block (Table 2).

### 5.2 Flow Conditions

Another key is determining if flow conditions may be represented in a pseudo-static manner or in a simplified dynamic sense (Figure 16). To do this, it is necessary to have an idea of the turbulent nature of the fluid motions in the vicinity of the rock mass being analyzed. Should flow be highly turbulent such that pressure applied to the rock mass fluctuates significantly, dynamic stability of removable blocks should be considered. If pressure fluctuations are relatively small, a pseudo-static treatment of the hydraulic load is adequate.

### 5.3 Hydrodynamic Pressure Distribution on Block

Probably the biggest unknown in the scour process is the 3D distribution of hydrodynamic pressures on the block faces. In light of limited data, it was assumed hydrodynamic pressures could be uniformly distributed over any combination of block faces, which for a tetrahedral block, yields 15 different combinations. For dynamic analysis, where the flow conditions can rapidly vary in orientation and

---

magnitude, all 15 hydraulic load scenarios should be considered to find the most critical load leading to removal of the block. Under pseudo-static conditions, however, it may be more appropriate to analyze a reduced set of load scenarios as a result of having, for example, a preferential flow direction. The later was implemented for the case study of the unlined spillway in northern California. It should be noted, the assumption of uniform pressure distribution on block faces is likely valid only for blocks smaller than the characteristic length scale of large-scale eddies within the flow. For larger blocks, this may be too conservative.

## **5.4 Block Stability**

Finally, stability of removable blocks was evaluated for lifting, 1-plane sliding and 2-plane sliding. Only stability for the pure translations was considered because the orientation of the active resultant is assumed to potentially vary in all directions. As such, the most critical mode will almost always be one of the translations unless the friction angle of the rock joint is very high.

Dynamic stability can be assessed by calculating block displacement in response to a characteristic pressure impulse (Figure 16). To do so, a failure criterion relating the amount of displacement to block removal is needed. Bollaert & Schleiss (2005) and Asadollahi (2009) provide a constant criteria for rectangular and cubic blocks relating the uplift to the vertical block dimension, however, it is hypothesized this criteria will be different (and variable) when considering blocks of different shapes and other failure modes. No criteria was developed from this analysis.

Pseudo-static stability can be assessed in the more traditional sense on which block theory was developed using limit equilibrium analysis. Analysis may be performed graphically (Figure 19) or using vector equations (Figure 18). For the case study of the unlined spillway, the later was preferred. Hydraulic pressures applied to the block were related to channel flow velocity based on research from the USBR (2007) on hydraulic jacking. Accordingly, block stability was determined for lifting and sliding as a function of flow velocity. As indicated in Table 2, critical flow velocities ranged between 4.4 m/s and 11.9 m/s, with some blocks having no feasible kinematic failure mode. This shows the influence of discontinuity orientation on block removability.

Furthermore, determination of the critical hydraulic load was highly dependent on block shape and orientation of the block faces. As such, the minimum hydrodynamic pressure causing removal did not usually produce an active resultant path that was shortest in distance to the limit equilibrium contour line (in the case of static analysis). Critical resultant paths were more influenced by a block face(s) that was relatively larger in area than the other block faces and that had a block side normal vector that plotted outside the limit equilibrium contour on the stereonet. Conversely, if pressure is applied to a block face that has a block side normal vector that plots inside of the limit equilibrium contour, the block may always be safe because as the pressure is increased, the active resultant forces aligns with

---

the block side normal vector (Figure 19 for pressure applied on J3). This result was anticipated as the active resultant force applied to the blocks is dominated by surficial water forces.

## **5.5 Implications**

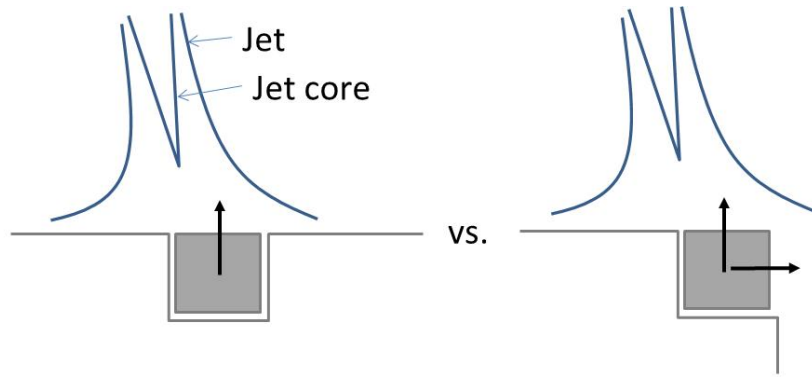
The use of block theory in scour assessment has several implications. Primarily, more accurate predictions of scour are achievable as the site-specific 3D geologic structure is accounted for. Additionally, with detailed field mapping, blocks most susceptible to scour can be targeted such that more efficient remediation measures can be implemented thus potentially reducing costs. Finally, analyses may be used as a planning tool for future projects to determine the most optimal layout of new spillways, for example, that are least susceptible to scour.

---

## 6. Recommendations for Further Study

During the development of this research a few areas were identified that merit further investigation. These are described below:

1. Hydrodynamic pressure distribution around block – Very little data exists regarding the 3D distribution of pressure on block faces and accordingly it is recommended to investigate how this changes over time for varying degrees of flow turbulence. This can probably be most readily done through physical hydraulic model testing. Obtaining such data will also give valuable insight on how 3D non-rectangular blocks interact and are removed when subject to hydraulic loads.
2. Verification of predicted critical flow velocities – It is recommended to collect additional field and laboratory data for a wide range of flow conditions to verify predictions made for critical flow velocities using the methodologies developed as part of this research.
3. Block free faces – The current research was limited to analyzing tetrahedral blocks with a single free face (such as those observed in the spillway channel bottom). Other blocks with multiple free faces were also observed in the spillway. It is recommended to extend analysis to these block types as well.
4. Block/flow geometry and relevance of pressure fluctuations on removal – For this analysis, a block in a highly turbulent flow field was recommended to be analyzed in a dynamic manner. However, for particular block geometries (such as a block with multiple free faces), the need to consider pressure fluctuations may not be relevant. Consider the simple 2D example of two blocks subject to an impinging jet: the first is a rectangular block in a rock mass flush with the surface (as is commonly tested in experimental set-ups, Fiorotto & Rinaldo 1992, Bollaert 2002, Federspiel et al. 2009 and others), and the second is a rectangular block on the edge of a rock mass. In the first case, the block is limited to translation in the vertical direction and the jet actually provides a stabilizing force. Only if the jet is turbulent and yields pressure fluctuations of sufficient duration, can the block be ejected. For the second case, however, the block can also readily translate into the free space at the right, while the same jet now provides a destabilizing force. In this scenario, the force imbalance on the block causing displacement is dominated by the geometry and any pressure fluctuations in the flow are of secondary concern for block removal (Figure 29). Therefore it may not be necessary to perform a dynamic analysis even in some flow situations that are highly turbulent.



Stabilizing jet in vertical direction

De-stabilizing jet in horizontal direction

Stabilizing jet in vertical direction

Figure 29: Example of block geometry dictating importance of pressure fluctuations for block removal.

---

## 7. References

- Achterberg, D., et al. 1998. Federal Guidelines for Dam Safety: Selecting and Accommodating Inflow Design Floods for Dams. FEMA 94.
- Annandale, G.W. 1995. Erodibility. *J. of Hyd. Research*. 33: 471-494.
- Annandale, G.W. 2006. Scour Technology. 1<sup>st</sup> ed. McGraw-Hill. New York.
- Asadollahi, P. 2009. Stability analysis of a single three dimensional rock block: effect of dilatancy and high-velocity water jet impact. Ph.D. Thesis, Dept. of Civil Engineering, Univ. of Texas, Austin.
- Atkinson, B.K. 1987. Fracture Mechanics of Rock. London: Academic Press.
- Barton, N., R. Lein, and J. Lunde. 1974. Engineering classification of rock masses for the design of tunnel support. *Rock Mechanics*. 6: 189-236.
- Barton, N., 1988. Rock mass classification and tunnel reinforcement selection using the Q-System: in Rock Classification Systems for Engineering Purposes: ASTM STP-984. Kirkaldie, L (Ed.). American Society for Testing and Materials. Philadelphia. 59-88.
- Bollaert, E., and A. Schleiss. 2005. Physically based model for evaluation of rock scour due to high-velocity jet impact. *J. of Hyd. Eng.* 131(3), 153-165.
- Bollaert, E. 2002. Transient Water Pressures in Joints and Formation of Rock Scour due to High-Velocity Jet Impact, *Communication No. 13*. Laboratory of Hydr. Constructions, Ecole Polytechnique Federale de Lausanne, Switzerland.
- Bollaert, E. 2010. Numerical modeling of scour at bridge foundations on rock. *Proc. from the 5<sup>th</sup> Int. Conf. on Scour and Erosion*. San Francisco, CA.
- Castillo, L.G., Puertas, J. and J. Dolz. 2007. Contribution to discussion of Bollaert and Schleiss' paper "Scour of rock due to the impact of plunging jet Part 1: A state-of-the-art review". *J. of Hyd. Research*. 45: 853-858.
- Dasgupta, B., Basu, D., Das, K., and Green, R. 2011. Development of computational methodology to assess erosion damage in dam spillways. *Proc. from the 31<sup>st</sup> Annual United States Society on Dam Conference*, San Diego, CA, April 11-15.
- Emmerling, R. 1973. The instantaneous of the wall pressure under a turbulent boundary layer flow. *Report No. 9*, Max-Planck-Institut fur Stromungsforschung.
- Ervine, D.A., and Falvey, H.R. 1987. Behavior of turbulent jets in the atmosphere and in plunge pools. *Proc. from the Inst. Of Civil Engineers*. 83(2), 295-314.
- Ervine, D.A., Falvey, H., & Withers, W. 1997. Pressure Fluctuations on Plunge Pool Floors. *J. of Hyd. Research* 35: 257-279.
- Federspiel, M., Bollaert, E., & Schleiss, A. 2009. Response of an intelligent block to symmetrical core jet impact. *Proc. from the 33<sup>rd</sup> IAHR Congress*, Vancouver, BC.
- Federspiel, M., Bollaert, E., & Schleiss, A. 2011. Dynamic response of a rock block in a plunge pool due to asymmetrical impact of a high-velocity jet. *Proc. from the 34<sup>rd</sup> IAHR Congress*, Brisbane, Australia.
- Fiorotto, V. and Rinaldo, A. 1992. Fluctuating uplift and lining design in spillway stilling basins. *J. of Hyd. Eng.*, 118:4, 578-596.
- George, M. F., and G. W. Annandale. 2006. Dam Failure by Rock Scour. *Proc. from the 41<sup>st</sup> U. S. Symposium on Rock Mechanics*. Golden, CO June 17 – 21.
- George, M. F. 2010. Private consulting report prepared for Freeport McMoRan Copper & Gold.

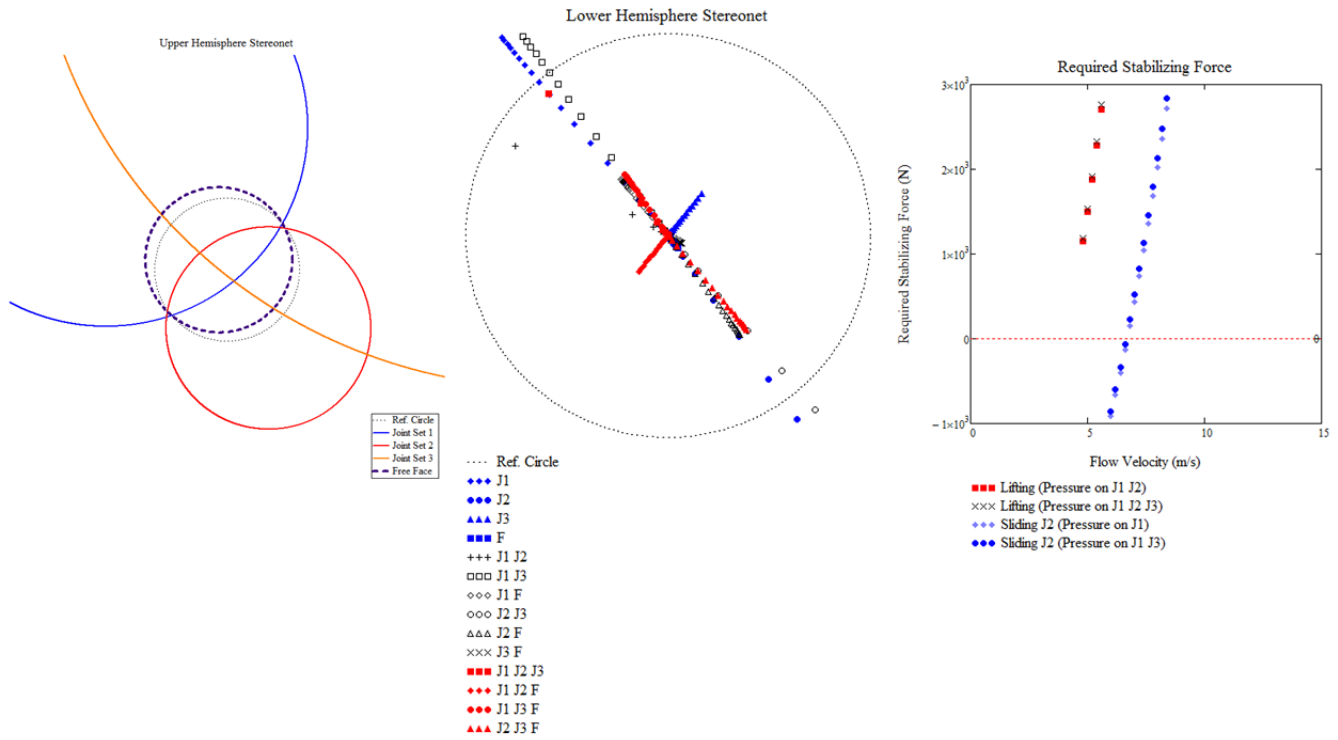
- 
- George, M.F. 2012. Scour of Discontinuous Blocky Rock. CE299 Report submitted in partial satisfaction for the Master of Science degree. University of California – Berkeley.
- Goodman, R.E. 1976. Methods of Geological Engineering in Discontinuous Rocks. West Publishing Company. St. Paul.
- Goodman, R. E., and Shi, G. 1985. Block Theory and Its Application to Rock Engineering. Prentice Hall. Englewood Cliffs, N.J.
- Goodman, R. E. and Y. Hatzor. 1991. Kendrick Project, Wyoming - Safety of Dam Deficiencies due to Overtopping: Results of Preliminary Analysis of Abutments Stability Based on Block Theory and the Critical Key Block Concept. Submitted to the USBR, Missouri Basin Region.
- Goodman, R.E. 1995. Block theory and its application. *Geotechnique* 45:3, 383-423.
- Goodman, R.E., and Powell, C. 2003. Investigations of blocks in foundations and abutments of concrete dams. *J. Geotech. and Geoenviron. Eng.* 129(2), 105-116.
- Grohmann, C. and Campanha, G. 2011. OpenStereo open source software for structural geology analysis.
- Hatzor, Y. 1992. Validation of Block Theory using field case histories. Ph.D. Thesis, Dept. of Civil Engineering, University of California, Berkeley.
- Hinze, J.D. 1975. Turbulence. 2<sup>nd</sup> ed. McGraw-Hill. New York.
- Kirsten, H.A.D., 1982. A classification system for excavation in natural materials. *The Civil Engineer in South Africa*. July. 292-308.
- Kirsten, H.A.D., 1988. Case histories of groundmass characterization for excavatability in Rock Classification Systems for Engineering Purposes. ASTM STP-984. Kirkaldie, L (Ed.). American Society for Testing and Materials. Philadelphia. 189-236.
- Li, A. and Liu, P. 2010. Mechanism of rock-bed scour due to impinging jet. *J. of Hyd. Research*, 48:1, 14-22.
- Manso, P. 2006. The influence of pool geometry and induced flow patterns in rock scour by high-velocity plunging jets, *Communication 25*, Laboratory of Hydraulic Constructions, Laboratory of Hydr. Constructions, Ecole Polytechnique Federale de Lausanne, Switzerland.
- Martins, R. 1973. Contribution to the knowledge on the scour action of free jets on rocky river beds. *Proc. from the 11<sup>th</sup> Congress on Large Dams*. Madrid, 799-814.
- Mauldon, M. 1990. Technical note: Probability aspects of the removability and rotatability of tetrahedral blocks, *Int. J. of Rock Mech, Min. Sci. and Geomech. Abst*, 27:4, 303-307.
- Mauldon, M. and Goodman, R. 1996. Vector analysis of keyblock rotations. *J. of Geotech. Eng.*, 122:12, 976-987.
- Melo, J.F., Pinheiro, A.N., Ramos, C.M. 2006. Forces on plunge pool slabs: influence of joints location and width, *J. of Hyd. Eng.*, 132:1, 49-60.
- Meshlab. 2011. Meshlab v1.3.0a. Open source software for 3D mesh processing and editing. Meshlab.sourceforge.net.
- PanTechnica Corp. 2002. KbSlope slope stability program for keyblock analysis. PanTechnica Corporation, Caska, MN.
- Paris, P.C., M.P. Gomez, W.E. Anderson. 1961. *Trend Engineering*. 13: 9-14.
- Reinius. 1986. Rock Erosion. *Water Power and Dam Construction*, June, 43-48.
- Tonon, F. 1998. Generalization of Mauldon's and Goodman's vector analysis of keyblock rotations. *J. of Geotech. and Geoenviron. Eng.* 124(10), 913-922.
-

- 
- Tonon, F. 2007. Analysis of single rock blocks for general failure modes under conservative and non-conservative forces. *Int. J. for Num. and Analytical Methods in Geomech.*, 31:1567-1608,
- Wibowo, J. L., and J. S. Lin. 2009. Stability Analysis of Spillways: Toward a Computational Approach. Powerpoint presentation taken from the internet.
- USBR (2007). Uplift and crack flow resulting from high velocity discharges over open offset joints. *Report DSO-07-07*, United States Bureau of Reclamation, Denver.
- Yuditskii, G.A. 1967. Actual pressure on the channel bottom below ski-jump spillways. *Izvestiya Vsesoyuznogo Nauchno-Issledovatel-Skogo Instuta Gidrotekhiki*, 67:231-240 (in Russian).

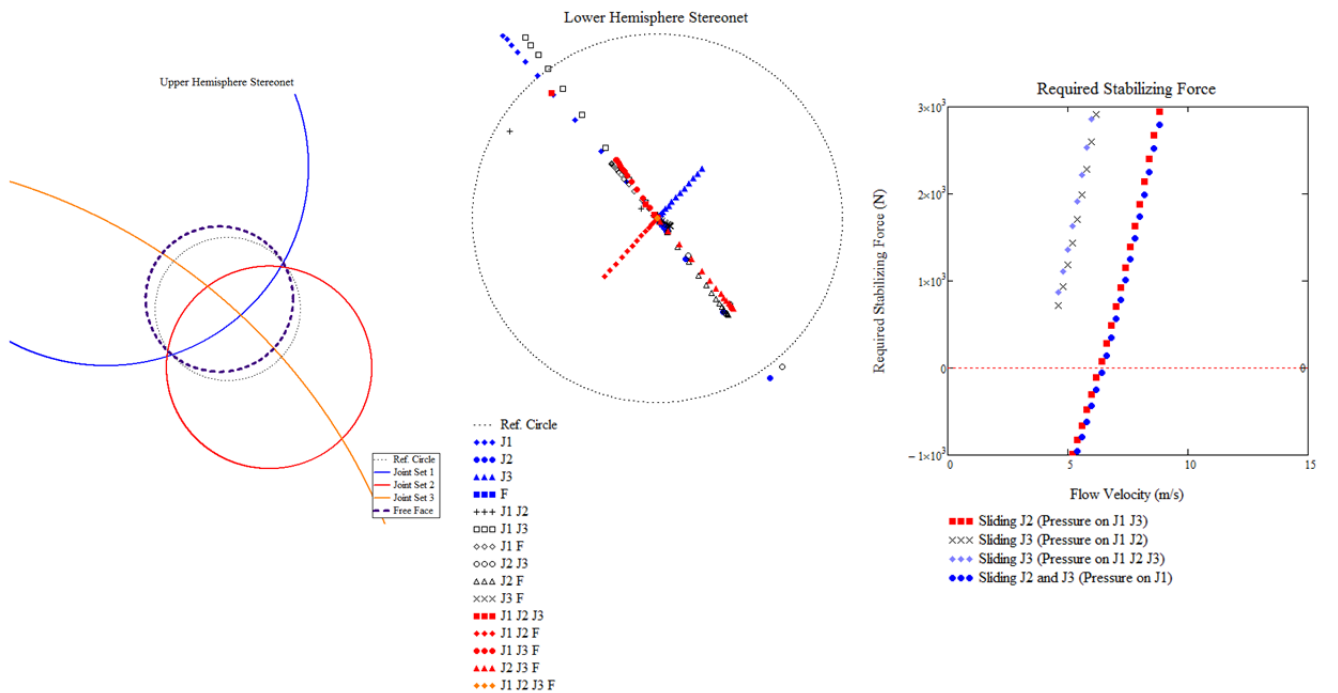
---

## **Appendix A: Additional results and calculations**

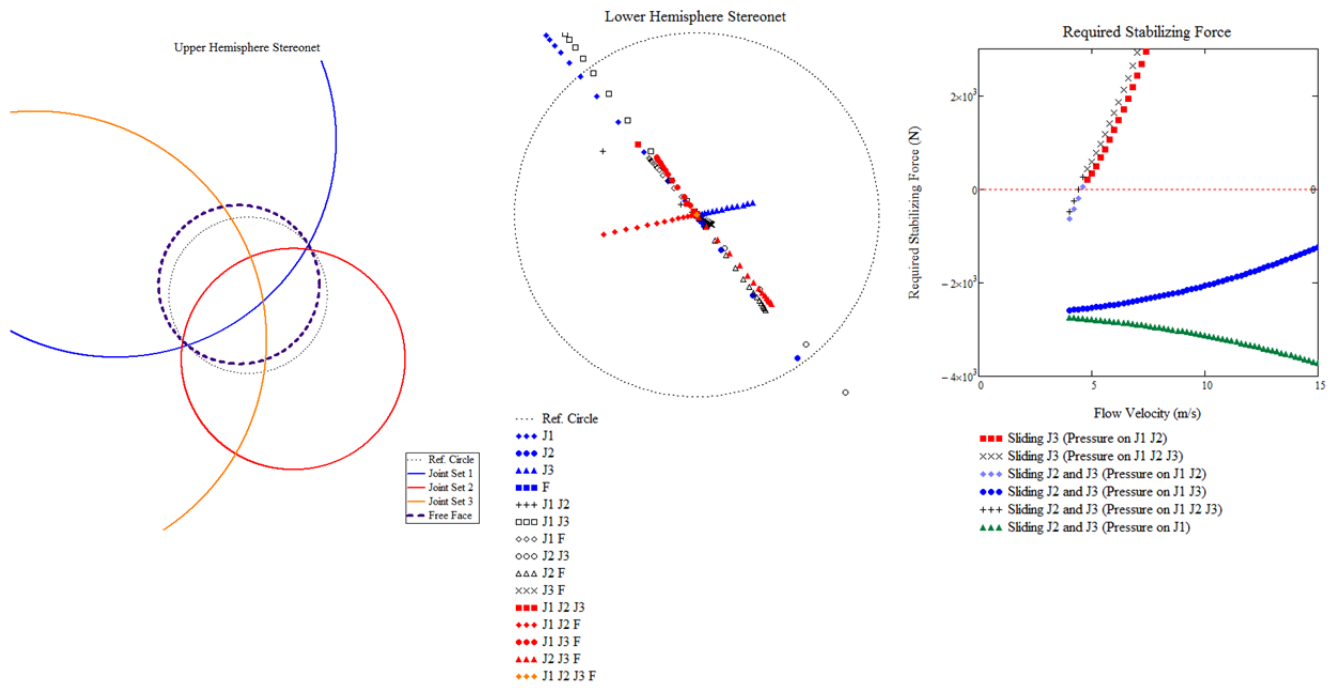
Hydraulic Load Scenario 1 (J1-J2-J3-F), (Stereonet for removability, Resultant paths plot, Stability plot)



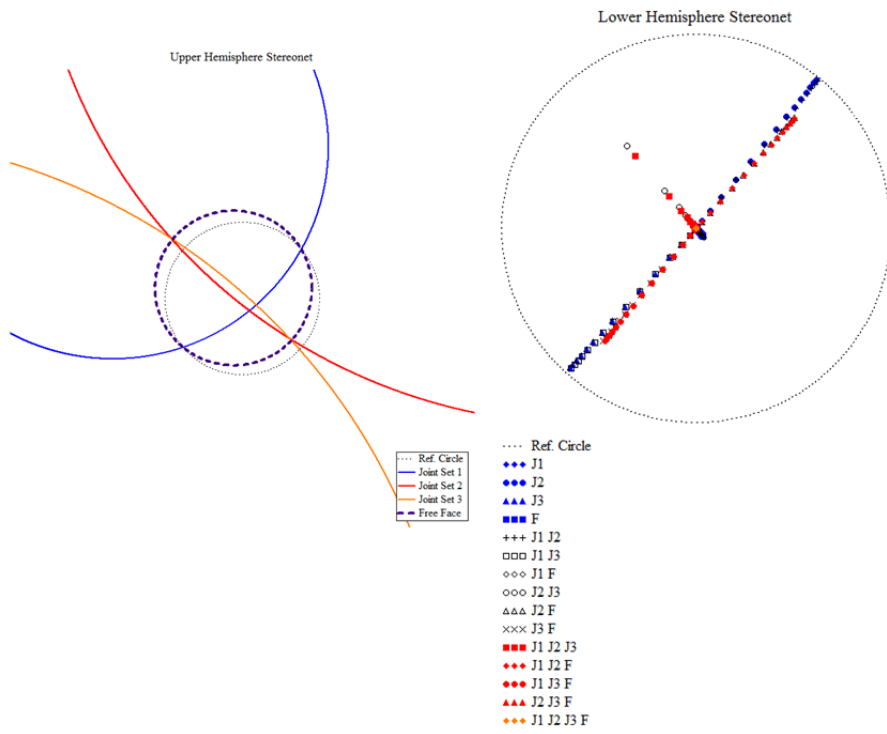
Hydraulic Load Scenario 2 (J1-J2-J4-F), (Stereonet for removability, Resultant paths plot, Stability plot)



Hydraulic Load Scenario 3 (J1-J2-J3-F) (Stereonet for removability, Resultant paths plot, Stability plot)

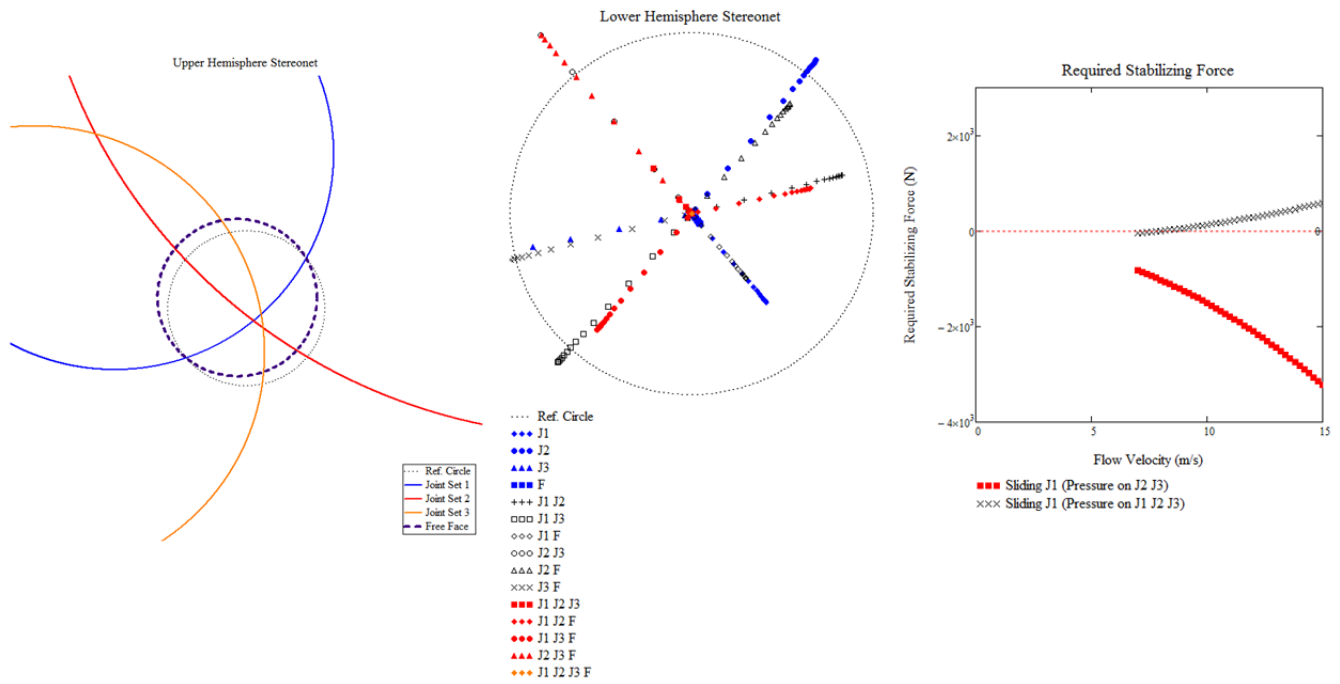


Hydraulic Load Scenario 4 (J1-J2-J3-F) (Stereonet for removability, Resultant paths plot, Stability plot)

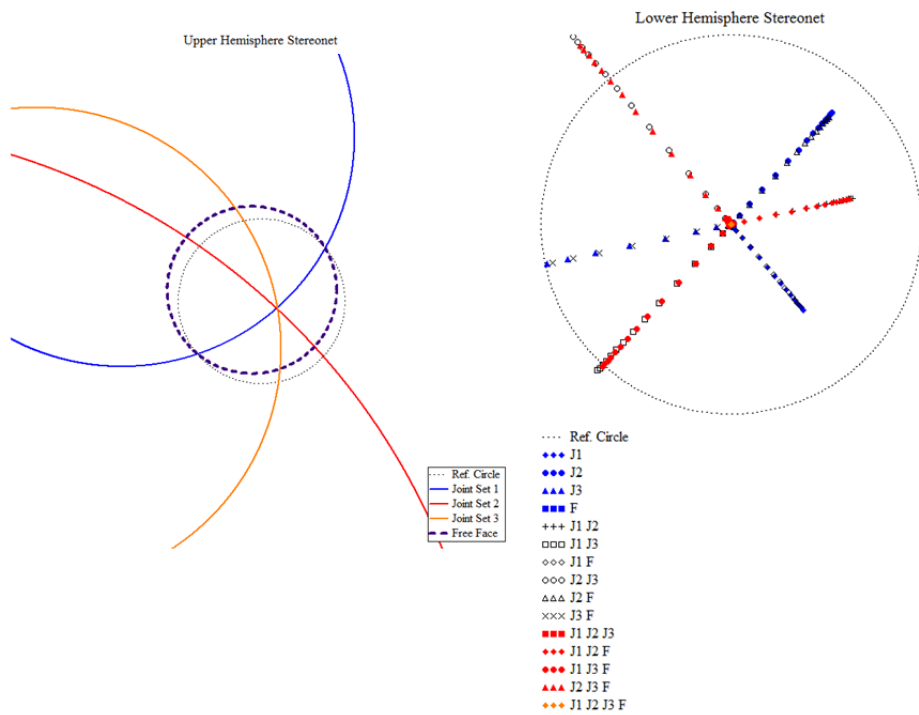


No unstable blocks

Hydraulic Load Scenario 5 (J1-J3-J5-F) (Stereonet for removability, Resultant paths plot, Stability plot)

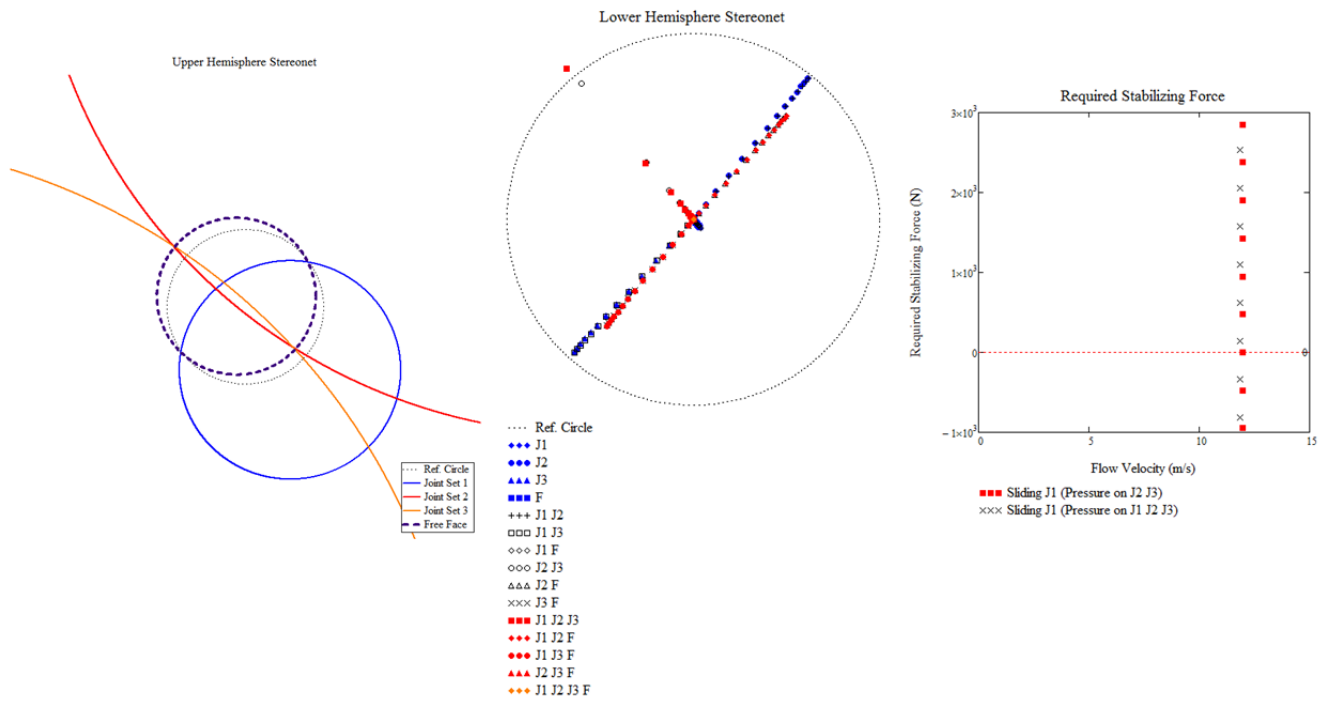


Hydraulic Load Scenario 6 (J1-J4-J5-F) (Stereonet for removability, Resultant paths plot, Stability plot)

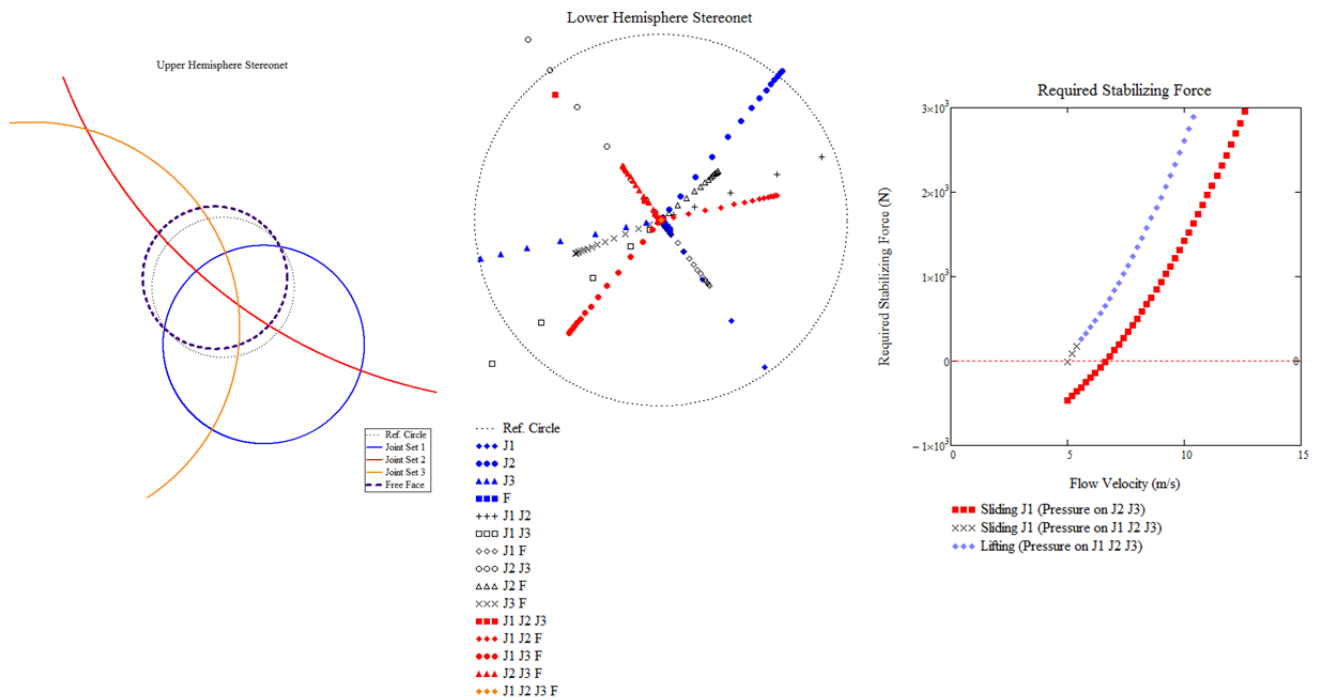


No unstable blocks

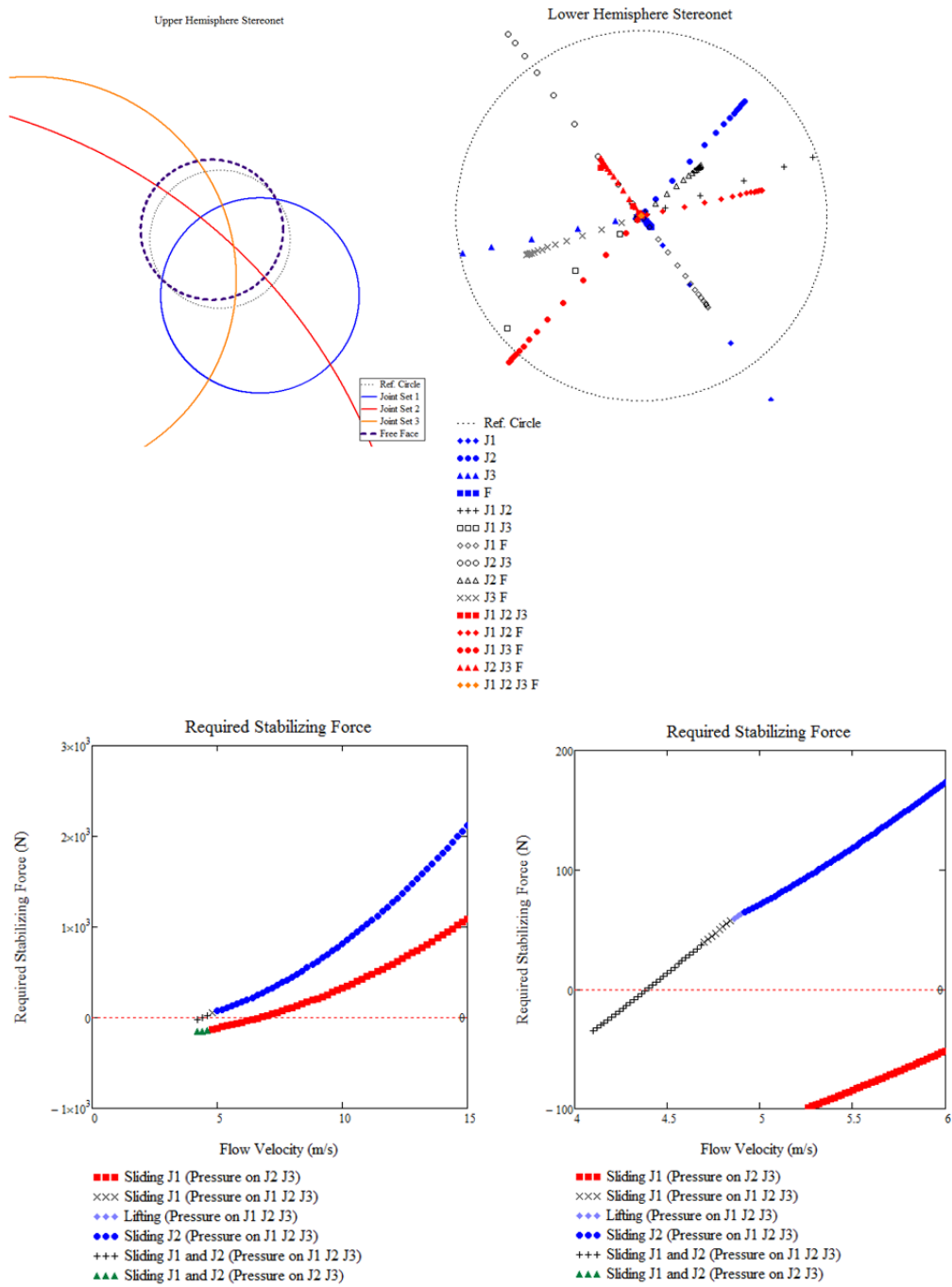
Hydraulic Load Scenario 7 (J2-J3-J4-F) (Stereonet for removability, Resultant paths plot, Stability plot)



Hydraulic Load Scenario 8 (J2-J3-J5-F) (Stereonet for removability, Resultant paths plot, Stability plot)

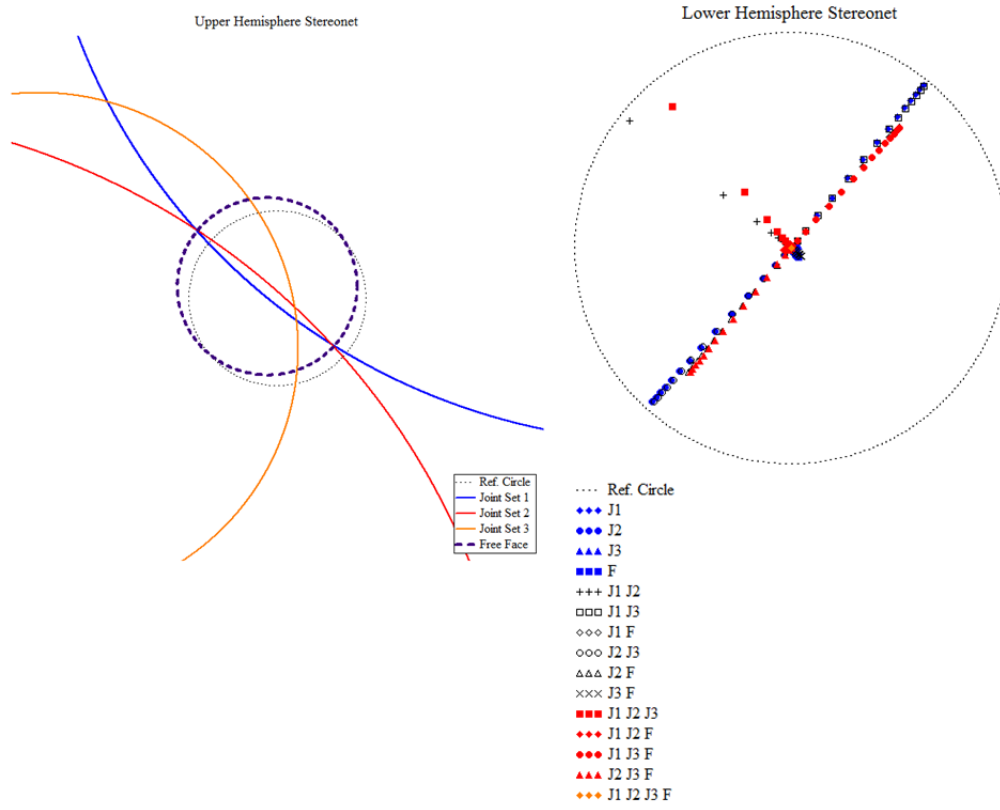


Hydraulic Load Scenario 9 (J2-J4-J5-F) (Stereonet for removability, Resultant paths plot, Stability plot)



(detail)

Hydraulic Load Scenario 10 (J3-J4-J5-F) (Stereonet for removability, Resultant paths plot, Stability plot)



No unstable blocks

# BLOCK THEORY ANALYSIS for ROCK SCOUR EVALUATION

By: MFG Date: 5/4/12

Calculations to analyze removability/rotatability, mode and stability of rock blocks subject to water pressures:

## INPUT

Dip	Dip Direction	Average Joint Spacing	
$\alpha := \begin{pmatrix} 69 \\ 45 \\ 82 \\ 10 \end{pmatrix} \cdot \text{deg}$	$\beta := \begin{pmatrix} 320 \\ 145 \\ 39 \\ 320 \end{pmatrix} \cdot \text{deg}$	$\delta := \begin{pmatrix} 3.4 \\ 1.6 \\ 3.4 \\ 1.5 \end{pmatrix} \cdot \text{ft}$	 User Input
		Free face	

$$\chi := \text{rows}(\alpha)$$

$$\rho_r := 2700 \frac{\text{kg}}{\text{m}^3} \quad \text{rock density}$$

$$\rho_w := 1000 \frac{\text{kg}}{\text{m}^3} \quad \text{water density}$$

$$\phi := 40 \text{deg} \quad \text{friction angle for joint planes (assumed)}$$

## REMOVABILITY & ROTATBILITY

### Stereonet Construction

Reference circle

$$R_{rc} := 1 \quad \text{Arbitrary radius of reference circle}$$

$$x_{rc}(\theta, R_{rc}) := R_{rc} \cdot \cos(\theta)$$

$$y_{rc}(\theta, R_{rc}) := R_{rc} \cdot \sin(\theta)$$

Great Circles

$$r(\alpha, R_{rc}) := \frac{R_{rc}}{\cos(\alpha)}$$

$$x(\alpha, R_{rc}, \theta) := r(\alpha, R_{rc}) \cdot \cos(\theta) + R_{rc} \cdot \tan(\alpha)$$

$$y(\alpha, R_{rc}, \theta) := r(\alpha, R_{rc}) \cdot \sin(\theta)$$

Great Circles for Joint Planes ( $\alpha' = \text{dip}$ ,  $\beta' = \text{dip direction}$ ) - UPPER hemisphere projection

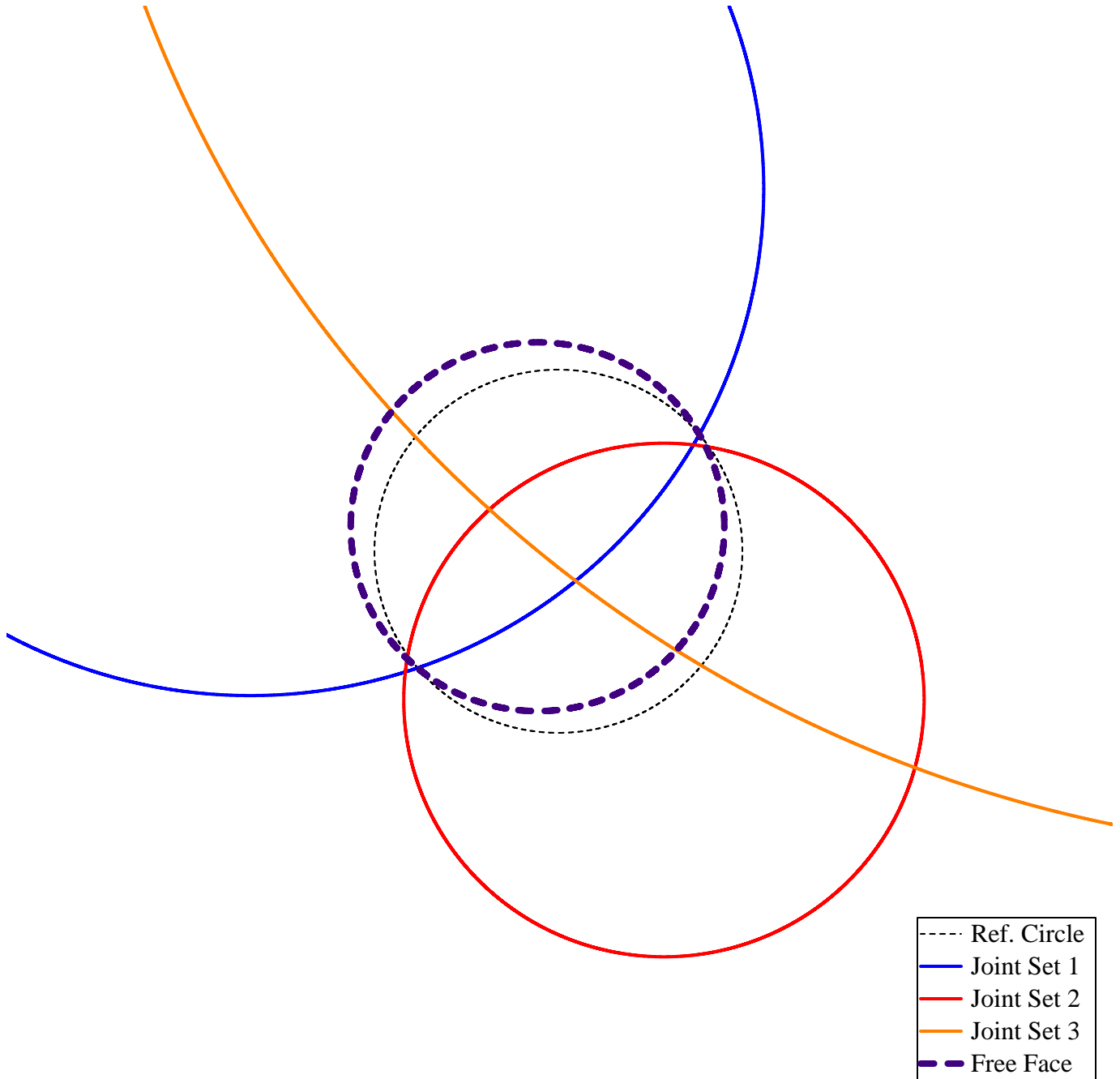
$$x''(\alpha', \beta', R_{rc}, \theta) := r(\alpha', R_{rc}) \cdot \cos(\theta) + R_{rc} \cdot \tan(\alpha') \cdot \cos\left(\frac{\pi}{2} - \beta'\right)$$

$$y''(\alpha', \beta', R_{rc}, \theta) := r(\alpha', R_{rc}) \cdot \sin(\theta) + R_{rc} \cdot \tan(\alpha') \cdot \sin\left(\frac{\pi}{2} - \beta'\right)$$

For lower hemisphere projection use  $3\pi/2 - \beta'$

$$\theta := 0, 0.0001 \dots 2\pi$$

# Upper Hemisphere Stereonet



Removal able blocks are those which plot inside the space pyramid (SP). The SP is the region to which blocks may move into. The excavation pyramid (EP) is the region where the blocks reside (i.e., the rock mass)

For this case the space pyramid is the space that is above the free surface (i.e., area inside the great circle corresponding to the free face). Conversely, the EP is the rock mass, which is space that is below the free surface (i.e., the area outside the great circle corresponding to the free face).

Compute normals to each plane:

$$\text{BC} := \begin{pmatrix} 0 \\ 0 \\ 0 \\ 1 \end{pmatrix} \begin{array}{l} \text{Full block code (including free face)} \\ \\ \\ \text{Free face} \end{array}$$

$$n := \begin{array}{l} i \leftarrow 1 \\ j \leftarrow 1 \\ \text{for } j \in 1 \dots \chi \\ \quad \text{for } i \in 1 \dots 3 \\ \quad \quad n_{i,j} \leftarrow \begin{cases} \sin(\alpha_j) \cdot \sin(\beta_j) & \text{if } i = 1 \\ \sin(\alpha_j) \cdot \cos(\beta_j) & \text{if } i = 2 \\ \cos(\alpha_j) & \text{otherwise} \end{cases} \\ \quad \quad i \leftarrow i + 1 \\ \quad i \leftarrow 1 \\ \quad j \leftarrow j + 1 \\ n \end{array}$$

$$n = \begin{pmatrix} -0.6 & 0.406 & 0.623 & -0.112 \\ 0.715 & -0.579 & 0.77 & 0.133 \\ 0.358 & 0.707 & 0.139 & 0.985 \end{pmatrix}$$

BLOCKSIDE Normals to each plane

$$n_b := \begin{array}{l} i \leftarrow 1 \\ j \leftarrow 1 \\ \text{for } j \in 1 \dots \chi \\ \quad \text{for } i \in 1 \dots 3 \\ \quad \quad n_{i,j} \leftarrow \begin{cases} \sin(\alpha_j) \cdot \sin(\beta_j) & \text{if } i = 1 \\ \sin(\alpha_j) \cdot \cos(\beta_j) & \text{if } i = 2 \\ \cos(\alpha_j) & \text{otherwise} \end{cases} \\ \quad \quad n_{i,j} \leftarrow \begin{cases} n_{i,j} & \text{if } \text{BC}_j = 0 \\ -n_{i,j} & \text{otherwise} \end{cases} \\ \quad \quad i \leftarrow i + 1 \\ \quad i \leftarrow 1 \\ \quad j \leftarrow j + 1 \\ n \end{array}$$

$$n_b = \begin{pmatrix} -0.6 & 0.406 & 0.623 & 0.112 \\ 0.715 & -0.579 & 0.77 & -0.133 \\ 0.358 & 0.707 & 0.139 & -0.985 \end{pmatrix}$$

Normals for planes used to calculate the coordinates of the block corners (i.e., the intersection of 3 planes) - See Goodman & Shi (1985) pg. 49, ex. 2.4

$$n_{123} := \begin{pmatrix} n_{1,1} & n_{2,1} & n_{3,1} \\ n_{1,2} & n_{2,2} & n_{3,2} \\ n_{1,3} & n_{2,3} & n_{3,3} \end{pmatrix} \quad n_{124} := \begin{pmatrix} n_{1,1} & n_{2,1} & n_{3,1} \\ n_{1,2} & n_{2,2} & n_{3,2} \\ n_{1,4} & n_{2,4} & n_{3,4} \end{pmatrix} \quad n_{134} := \begin{pmatrix} n_{1,1} & n_{2,1} & n_{3,1} \\ n_{1,3} & n_{2,3} & n_{3,3} \\ n_{1,4} & n_{2,4} & n_{3,4} \end{pmatrix} \quad n_{234} := \begin{pmatrix} n_{1,2} & n_{2,2} & n_{3,2} \\ n_{1,3} & n_{2,3} & n_{3,3} \\ n_{1,4} & n_{2,4} & n_{3,4} \end{pmatrix}$$

Distance from each joint plane to origin (input by user)

$$D := \begin{pmatrix} \frac{\delta_1}{3} \\ \frac{\delta_2}{3} \\ \frac{\delta_3}{3} \\ \frac{\delta_4}{3} \end{pmatrix}$$

Distances to planes used to calculate the coordinates of the block corners (i.e., the intersection of 3 planes) -  
 See Goodman & Shi (1985) pg. 49, ex. 2.4

$$D_{123} := \begin{pmatrix} D_1 \\ D_2 \\ D_3 \end{pmatrix} \quad D_{124} := \begin{pmatrix} D_1 \\ D_2 \\ D_4 \end{pmatrix} \quad D_{134} := \begin{pmatrix} D_1 \\ D_3 \\ D_4 \end{pmatrix} \quad D_{234} := \begin{pmatrix} D_2 \\ D_3 \\ D_4 \end{pmatrix}$$

Coordinates of block corners (X,Y,Z):

$$A1 := n_{124}^{-1} \cdot D_{124} = \begin{pmatrix} -4.308 \\ -3.18 \\ 0.096 \end{pmatrix} \text{ m} \quad A2 := n_{234}^{-1} \cdot D_{234} = \begin{pmatrix} 0.325 \\ 0.155 \\ 0.171 \end{pmatrix} \text{ m}$$

$$A3 := n_{134}^{-1} \cdot D_{134} = \begin{pmatrix} -2.068 \times 10^{-3} \\ 0.433 \\ 0.096 \end{pmatrix} \quad A4 := n_{123}^{-1} \cdot D_{123} = \begin{pmatrix} 0.066 \\ 0.314 \\ 0.449 \end{pmatrix} \text{ m}$$

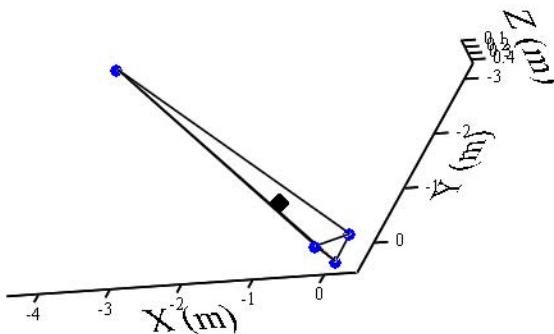
Points to plot tetrahedron

$$B := \begin{pmatrix} A1_1 & A1_2 & A1_3 \\ A2_1 & A2_2 & A2_3 \\ A3_1 & A3_2 & A3_3 \\ A4_1 & A4_2 & A4_3 \\ A1_1 & A1_2 & A1_3 \\ A3_1 & A3_2 & A3_3 \\ A4_1 & A4_2 & A4_3 \\ A2_1 & A2_2 & A2_3 \end{pmatrix}$$

The centroid of the tetrahedron is:

$$G_b := \frac{A1 + A2 + A3 + A4}{4} = \begin{pmatrix} -0.98 \\ -0.569 \\ 0.203 \end{pmatrix} \text{ m} \quad xG := (G_{b1}), yG := (G_{b2}), zG := (G_{b3})$$

Removable Block (showing Centroid)



$$(B^{(1)}, B^{(2)}, B^{(3)}), (xG, yG, zG)$$

$$V_b := \frac{1}{6} \cdot \left| \begin{pmatrix} 1 & \frac{A1_1}{m} & \frac{A1_2}{m} & \frac{A1_3}{m} \\ 1 & \frac{A2_1}{m} & \frac{A2_2}{m} & \frac{A2_3}{m} \\ 1 & \frac{A3_1}{m} & \frac{A3_2}{m} & \frac{A3_3}{m} \\ 1 & \frac{A4_1}{m} & \frac{A4_2}{m} & \frac{A4_3}{m} \end{pmatrix} \right| \cdot m^3 = 0.13 \cdot m^3$$

Mass of block

$$m_b := \rho_r \cdot V_b = 352.132 \text{ kg}$$

Area of block faces

$$A_b := \left[ \begin{aligned} & \frac{1}{2} \cdot \left[ \left[ \left( \frac{A3_2}{m} - \frac{A1_2}{m} \frac{A3_3}{m} - \frac{A1_3}{m} \right)^2 + \left( \frac{A3_3}{m} - \frac{A1_3}{m} \frac{A3_1}{m} - \frac{A1_1}{m} \right)^2 + \left( \frac{A3_1}{m} - \frac{A1_1}{m} \frac{A3_2}{m} - \frac{A1_2}{m} \right)^2 \right]^{\frac{1}{2}} \right. \\ & \frac{1}{2} \cdot \left[ \left[ \left( \frac{A2_2}{m} - \frac{A1_2}{m} \frac{A2_3}{m} - \frac{A1_3}{m} \right)^2 + \left( \frac{A2_3}{m} - \frac{A1_3}{m} \frac{A2_1}{m} - \frac{A1_1}{m} \right)^2 + \left( \frac{A2_1}{m} - \frac{A1_1}{m} \frac{A2_2}{m} - \frac{A1_2}{m} \right)^2 \right]^{\frac{1}{2}} \right. \\ & \frac{1}{2} \cdot \left[ \left[ \left( \frac{A3_2}{m} - \frac{A2_2}{m} \frac{A3_3}{m} - \frac{A2_3}{m} \right)^2 + \left( \frac{A3_3}{m} - \frac{A2_3}{m} \frac{A3_1}{m} - \frac{A2_1}{m} \right)^2 + \left( \frac{A3_1}{m} - \frac{A2_1}{m} \frac{A3_2}{m} - \frac{A2_2}{m} \right)^2 \right]^{\frac{1}{2}} \right. \\ & \left. \frac{1}{2} \cdot \left[ \left[ \left( \frac{A2_2}{m} - \frac{A1_2}{m} \frac{A2_3}{m} - \frac{A1_3}{m} \right)^2 + \left( \frac{A2_3}{m} - \frac{A1_3}{m} \frac{A2_1}{m} - \frac{A1_1}{m} \right)^2 + \left( \frac{A2_1}{m} - \frac{A1_1}{m} \frac{A2_2}{m} - \frac{A1_2}{m} \right)^2 \right]^{\frac{1}{2}} \right] \right] \cdot m \end{aligned}$$

$$A_b = \begin{pmatrix} 1.062 \\ 1.129 \\ 0.072 \\ 1.208 \end{pmatrix} m^2$$

- Face with corners A1, A3, A4 - Joint Plane 1
- Face with corners A1, A2, A4 - Joint Plane 2
- Face with corners A2, A3, A4 - Joint Plane 3
- Face with corners A1, A2, A3 - the free face

## Coordinates for Centroid Triangular Face

$$G_{134} := \frac{A1 + A3 + A4}{3} = \begin{pmatrix} -1.415 \\ -0.811 \\ 0.214 \end{pmatrix} \text{ m} \quad \text{Face with corners A1, A3, A4 - joint 1}$$

$$G_{124} := \frac{A1 + A2 + A4}{3} = \begin{pmatrix} -1.306 \\ -0.904 \\ 0.238 \end{pmatrix} \text{ m} \quad \text{Face with corners A1, A2, A4 - joint 2}$$

$$G_{234} := \frac{A2 + A3 + A4}{3} = \begin{pmatrix} 0.13 \\ 0.301 \\ 0.238 \end{pmatrix} \text{ m} \quad \text{Face with corners A2, A3, A4 - joint 3}$$

$$G_{123} := \frac{A1 + A2 + A3}{3} = \begin{pmatrix} -1.328 \\ -0.864 \\ 0.121 \end{pmatrix} \text{ m} \quad \text{Face with corners A1, A2, A3 - the free face}$$

## ACTIVE RESULTANT

### Self weight

$$W_b := m_b \cdot g$$

### Water Force

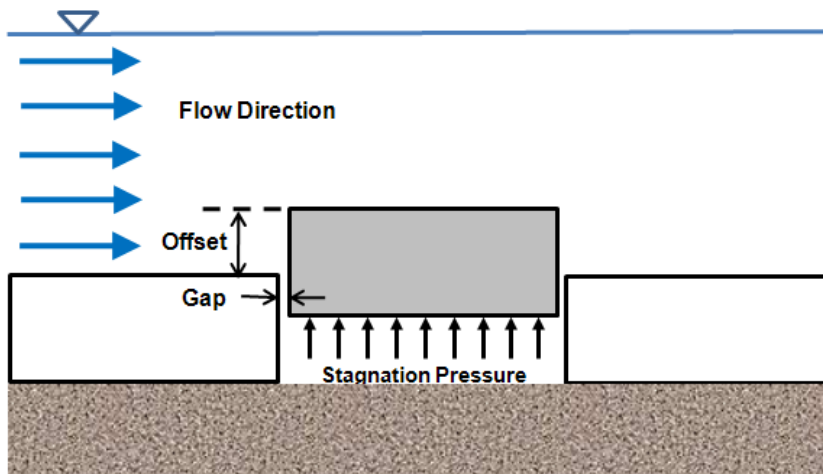
Energy coefficient (to increase or decrease pressure based on flow conditions)

$$\varphi := 1$$

For flow impacting a small perturbation of a block edge, stagnation pressure is created beneath the block. This pressure can be quantified using research from the Bureau of Reclamation in Denver, CO (2007). The generic formula for the uplift pressure head from stagnation is:

$$h = a \cdot v^b$$

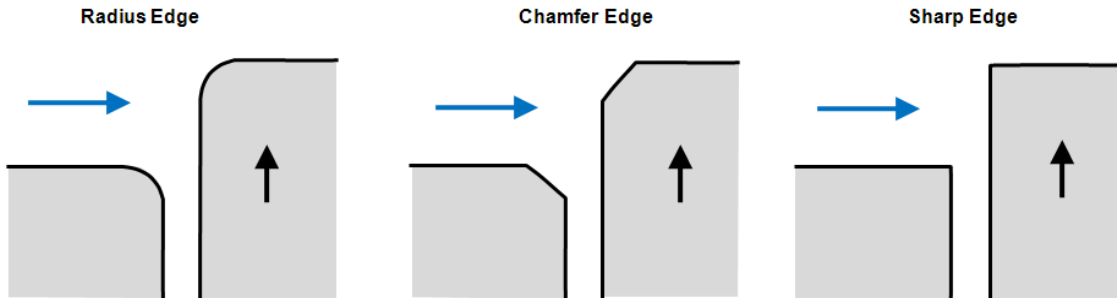
"a" and "b" are coefficients (see below)  
"v" is the flow velocity



**Gap := 0.125in** Spacing b/w blocks. Enter 0.125in, 0.25in or 0.5in

**Off := 0.125in** The offset is determined in the loop below (for  $\Delta z$ ) and is based on the initial uplift of the block when the block is flush with the surrounding blocks.

The block edge geometries tested by the BOR are as follows.



**Geometry := 1** Enter "1" for radius edge geometry - assumed for rock joints  
Enter "2" for chamfer edge geometry  
Enter "3" for sharp edge geometry

Values of "a" for various gap spacings and offsets for "sharp edge", "radius" and "chamfer" edge geometries. Values provided are for a VENTED block (i.e., the rock joints are open)

```
a_s_radius(Off) := 0 if Off = 0in
0.00387 if [(Gap = 0.125in) ^ (0in < Off ≤ 0.125in)]
0.00622 if [(Gap = 0.125in) ^ (0.125in < Off ≤ 0.25in)]
0.00790 if [(Gap = 0.125in) ^ (0.25in < Off ≤ 0.5in)]
0.01101 if [(Gap = 0.125in) ^ (Off > 0.5in)]
0.00333 if [(Gap = 0.25in) ^ (0 < Off ≤ 0.125in)]
0.00575 if [(Gap = 0.25in) ^ (0.125in < Off ≤ 0.25in)]
0.00838 if [(Gap = 0.25in) ^ (0.25in < Off ≤ 0.5in)]
0.00869 if [(Gap = 0.25in) ^ (Off > 0.5in)]
0.00253 if [(Gap = 0.5in) ^ (0 < Off ≤ 0.125in)]
0.00470 if [(Gap = 0.5in) ^ (0.125in < Off ≤ 0.25in)]
0.00614 if [(Gap = 0.5in) ^ (0.25in < Off ≤ 0.5in)]
0.00741 if [(Gap = 0.5in) ^ (Off > 0.5in)]
0 otherwise
```

$$a_{s\_chamfer}(Off) := \begin{cases} 0 & \text{if } Off = 0in \\ 0.00477 & \text{if } [(Gap = 0.125in) \wedge (0in < Off \leq 0.125in)] \\ 0.00629 & \text{if } [(Gap = 0.125in) \wedge (0.125in < Off \leq 0.25in)] \\ 0.01084 & \text{if } [(Gap = 0.125in) \wedge (0.25in < Off \leq 0.5in)] \\ 0.01355 & \text{if } [(Gap = 0.125in) \wedge (Off > 0.5in)] \\ 0.00316 & \text{if } [(Gap = 0.25in) \wedge (0 < Off \leq 0.125in)] \\ 0.00585 & \text{if } [(Gap = 0.25in) \wedge (0.125in < Off \leq 0.25in)] \\ 0.01019 & \text{if } [(Gap = 0.25in) \wedge (0.25in < Off \leq 0.5in)] \\ 0.01125 & \text{if } [(Gap = 0.25in) \wedge (Off > 0.5in)] \\ 0.00243 & \text{if } [(Gap = 0.5in) \wedge (0 < Off \leq 0.125in)] \\ 0.00478 & \text{if } [(Gap = 0.5in) \wedge (0.125in < Off \leq 0.25in)] \\ 0.00879 & \text{if } [(Gap = 0.5in) \wedge (0.25in < Off \leq 0.5in)] \\ 0.01056 & \text{if } [(Gap = 0.5in) \wedge (Off > 0.5in)] \\ 0 & \text{otherwise} \end{cases}$$

$$a_{s\_sharp}(Off) := \begin{cases} 0 & \text{if } Off = 0in \\ 0.00422 & \text{if } [(Gap = 0.125in) \wedge (0in < Off \leq 0.125in)] \\ 0.00707 & \text{if } [(Gap = 0.125in) \wedge (0.125in < Off \leq 0.25in)] \\ 0.01207 & \text{if } [(Gap = 0.125in) \wedge (0.25in < Off \leq 0.5in)] \\ 0.01599 & \text{if } [(Gap = 0.125in) \wedge (Off > 0.5in)] \\ 0.00308 & \text{if } [(Gap = 0.25in) \wedge (0 < Off \leq 0.125in)] \\ 0.00546 & \text{if } [(Gap = 0.25in) \wedge (0.125in < Off \leq 0.25in)] \\ 0.00994 & \text{if } [(Gap = 0.25in) \wedge (0.25in < Off \leq 0.5in)] \\ 0.00973 & \text{if } [(Gap = 0.25in) \wedge (Off > 0.5in)] \\ 0.00243 & \text{if } [(Gap = 0.5in) \wedge (0 < Off \leq 0.125in)] \\ 0.00420 & \text{if } [(Gap = 0.5in) \wedge (0.125in < Off \leq 0.25in)] \\ 0.00732 & \text{if } [(Gap = 0.5in) \wedge (0.25in < Off \leq 0.5in)] \\ 0.00909 & \text{if } [(Gap = 0.5in) \wedge (Off > 0.5in)] \\ 0 & \text{otherwise} \end{cases}$$

Determines correct "a" coefficient depending on geometry selected

$$a_s(Off) := \begin{cases} a_{s\_radius}(Off) & \text{if } Geometry = 1 \\ a_{s\_chamfer}(Off) & \text{if } Geometry = 2 \\ a_{s\_sharp}(Off) & \text{otherwise} \end{cases}$$

Values of "b" for various gap spacings and offsets for "sharp edge", "radius" and "chamfer" edge geometries. Values provided are for a VENTED block.

$b_{s\_radius}(Off) :=$ 

2.08813	if [(Gap = 0.125in) ∧ (Off ≤ 0.125in)]
2.04700	if [(Gap = 0.125in) ∧ (0.125in < Off ≤ 0.25in)]
2.03953	if [(Gap = 0.125in) ∧ (0.25in < Off ≤ 0.5in)]
1.98957	if [(Gap = 0.125in) ∧ (Off > 0.5in)]
2.04385	if [(Gap = 0.25in) ∧ (Off ≤ 0.125in)]
2.03262	if [(Gap = 0.25in) ∧ (0.125in < Off ≤ 0.25in)]
2.03420	if [(Gap = 0.25in) ∧ (0.25in < Off ≤ 0.5in)]
2.06829	if [(Gap = 0.25in) ∧ (Off > 0.5in)]
2.05472	if [(Gap = 0.5in) ∧ (Off ≤ 0.125in)]
2.02695	if [(Gap = 0.5in) ∧ (0.125in < Off ≤ 0.25in)]
2.07939	if [(Gap = 0.5in) ∧ (0.25in < Off ≤ 0.5in)]
2.09057	if [(Gap = 0.5in) ∧ (Off > 0.5in)]
0	otherwise

$b_{s\_chamfer}(Off) :=$ 

2.01598	if [(Gap = 0.125in) ∧ (Off ≤ 0.125in)]
2.05685	if [(Gap = 0.125in) ∧ (0.125in < Off ≤ 0.25in)]
1.96694	if [(Gap = 0.125in) ∧ (0.25in < Off ≤ 0.5in)]
1.94340	if [(Gap = 0.125in) ∧ (Off > 0.5in)]
2.03835	if [(Gap = 0.25in) ∧ (Off ≤ 0.125in)]
2.03202	if [(Gap = 0.25in) ∧ (0.125in < Off ≤ 0.25in)]
1.99466	if [(Gap = 0.25in) ∧ (0.25in < Off ≤ 0.5in)]
2.00847	if [(Gap = 0.25in) ∧ (Off > 0.5in)]
2.03809	if [(Gap = 0.5in) ∧ (Off ≤ 0.125in)]
2.02460	if [(Gap = 0.5in) ∧ (0.125in < Off ≤ 0.25in)]
1.99484	if [(Gap = 0.5in) ∧ (0.25in < Off ≤ 0.5in)]
2.00565	if [(Gap = 0.5in) ∧ (Off > 0.5in)]
0	otherwise

$b_{s\_sharp}(Off) :=$ 

2.08575	if [(Gap = 0.125in) ∧ (Off ≤ 0.125in)]
2.01796	if [(Gap = 0.125in) ∧ (0.125in < Off ≤ 0.25in)]
1.94415	if [(Gap = 0.125in) ∧ (0.25in < Off ≤ 0.5in)]
1.91156	if [(Gap = 0.125in) ∧ (Off > 0.5in)]
2.11373	if [(Gap = 0.25in) ∧ (Off ≤ 0.125in)]
2.08292	if [(Gap = 0.25in) ∧ (0.125in < Off ≤ 0.25in)]
2.00543	if [(Gap = 0.25in) ∧ (0.25in < Off ≤ 0.5in)]
2.05841	if [(Gap = 0.25in) ∧ (Off > 0.5in)]
2.07779	if [(Gap = 0.5in) ∧ (Off ≤ 0.125in)]
2.08693	if [(Gap = 0.5in) ∧ (0.125in < Off ≤ 0.25in)]
2.06328	if [(Gap = 0.5in) ∧ (0.25in < Off ≤ 0.5in)]
2.07265	if [(Gap = 0.5in) ∧ (Off > 0.5in)]
0	otherwise

Determines correct "b" coefficient depending on geometry selected.

$$b_s(\text{Off}) := \begin{cases} b_{s\_radius}(\text{Off}) & \text{if Geometry} = 1 \\ b_{s\_chamfer}(\text{Off}) & \text{if Geometry} = 2 \\ b_{s\_sharp}(\text{Off}) & \text{otherwise} \end{cases}$$

Using the coefficients above, the pressure head associated with the stagnation pressure is:

$$h'_s(v, \text{Off}) := a_s(\text{Off}) \cdot \left( \frac{v}{0.3048 \text{ SIUnitsOf}(v)} \right)^{b_s(\text{Off})} \cdot \text{ft}$$

Units of "h'<sub>s</sub>" must be "ft" based on BOR relationship. (MathCAD default units are "m", so must strip "m" unit, divide by 0.3048 to convert to "ft" and re-apply units of "ft")

The following function is written to linear interpolated values of "h'<sub>s</sub>" when the "offset" is between the tested values.

$$h'_s(v, \text{Off}) := \begin{cases} h'_s(v, 0\text{in}) & \text{if Off} = 0\text{in} \\ \left[ \left( \frac{\text{Off} - 0\text{in}}{0.125\text{in} - 0\text{in}} \right) \cdot (h'_s(v, 0.125\text{in}) - h'_s(v, 0\text{in})) + h'_s(v, 0\text{in}) \right] & \text{if } 0\text{in} < \text{Off} < 0.125\text{in} \\ h'_s(v, 0.125\text{in}) & \text{if Off} = 0.125\text{in} \\ \left[ \left( \frac{\text{Off} - 0.125\text{in}}{0.25\text{in} - 0.125\text{in}} \right) \cdot (h'_s(v, 0.25\text{in}) - h'_s(v, 0.125\text{in})) + h'_s(v, 0.125\text{in}) \right] & \text{if } 0.125\text{in} < \text{Off} < 0.25\text{in} \\ h'_s(v, 0.25\text{in}) & \text{if Off} = 0.25\text{in} \\ \left[ \left( \frac{\text{Off} - 0.25\text{in}}{0.5\text{in} - 0.25\text{in}} \right) \cdot (h'_s(v, 0.5\text{in}) - h'_s(v, 0.25\text{in})) + h'_s(v, 0.25\text{in}) \right] & \text{if } 0.25\text{in} < \text{Off} < 0.5\text{in} \\ h'_s(v, 0.5\text{in}) & \text{if Off} = 0.5\text{in} \\ \left[ \left( \frac{\text{Off} - 0.5\text{in}}{0.75\text{in} - 0.5\text{in}} \right) \cdot (h'_s(v, 0.75\text{in}) - h'_s(v, 0.5\text{in})) + h'_s(v, 0.5\text{in}) \right] & \text{if } 0.5\text{in} < \text{Off} < 0.75\text{in} \\ h'_s(v, 0.75\text{in}) & \text{otherwise} \end{cases}$$

Convert to pressure:

$$P_s(v, \text{Off}) := h'_s(v, \text{Off}) \cdot \gamma$$

The components of the water force in the x, y and z directions are expressed below. The values of h, i, j, k (corresponding to joints 1, 2, 3 and the free face, respectively) either have a value of "1" or "0" indicating whether or not the joint plane is used in the determination of the hydraulic load applied to the block. For a tetrahedral block, it is assumed water pressures can be applied to any combination of the joint faces (this is likely reasonable to account for the transient nature of pressures occurring in rock joints). For example, if h = 0, i = 0, j = 1 and k = 1 then the water pressure is assumed to be applied evenly over joint 3 and the free face.

$$F_{W\_x}(v, h, i, j, k) := \varphi \cdot \rho_w \cdot (g \cdot h'_s(v, \text{Off})) \cdot \left[ \left( n_b^{(1)} \right)_1 \cdot (A_{b_1} \cdot h) + \left( n_b^{(2)} \right)_1 \cdot (A_{b_2} \cdot i) + \left( n_b^{(3)} \right)_1 \cdot (A_{b_3} \cdot j) + \left( n_b^{(4)} \right)_1 \cdot (A_{b_4} \cdot k) \right]$$

$$F_{W\_y}(v, h, i, j, k) := \varphi \cdot \rho_w \cdot (g \cdot h_s(v, \text{Off})) \cdot \left[ \left( n_b^{(1)} \right)_2 \cdot (A_{b_1} \cdot h) + \left( n_b^{(2)} \right)_2 \cdot (A_{b_2} \cdot i) + \left( n_b^{(3)} \right)_2 \cdot (A_{b_3} \cdot j) + \left( n_b^{(4)} \right)_2 \cdot (A_{b_4} \cdot k) \right]$$

$$F_{W\_z}(v, h, i, j, k) := \varphi \cdot \rho_w \cdot (g \cdot h_s(v, \text{Off})) \cdot \left[ \left( n_b^{(1)} \right)_3 \cdot (A_{b_1} \cdot h) + \left( n_b^{(2)} \right)_3 \cdot (A_{b_2} \cdot i) + \left( n_b^{(3)} \right)_3 \cdot (A_{b_3} \cdot j) + \left( n_b^{(4)} \right)_3 \cdot (A_{b_4} \cdot k) \right]$$

The active resultant force in the x, y and z directions

$$R_{a\_x}(v, h, i, j, k) := F_{W\_x}(v, h, i, j, k)$$

$$R_{a\_y}(v, h, i, j, k) := F_{W\_y}(v, h, i, j, k)$$

$$R_{a\_z}(v, h, i, j, k) := F_{W\_z}(v, h, i, j, k) - W_b$$

Unit active resultant

$$r_{a\_x}(v, h, i, j, k) := \frac{R_{a\_x}(v, h, i, j, k)}{\sqrt{R_{a\_x}(v, h, i, j, k)^2 + R_{a\_y}(v, h, i, j, k)^2 + R_{a\_z}(v, h, i, j, k)^2}}$$

$$r_{a\_y}(v, h, i, j, k) := \frac{R_{a\_y}(v, h, i, j, k)}{\sqrt{R_{a\_x}(v, h, i, j, k)^2 + R_{a\_y}(v, h, i, j, k)^2 + R_{a\_z}(v, h, i, j, k)^2}}$$

$$r_{a\_z}(v, h, i, j, k) := \frac{R_{a\_z}(v, h, i, j, k)}{\sqrt{R_{a\_x}(v, h, i, j, k)^2 + R_{a\_y}(v, h, i, j, k)^2 + R_{a\_z}(v, h, i, j, k)^2}}$$

Put active resultant components into vector form

$$r_a(v, h, i, j, k) := \begin{pmatrix} r_{a\_x}(v, h, i, j, k) \\ r_{a\_y}(v, h, i, j, k) \\ r_{a\_z}(v, h, i, j, k) \end{pmatrix} \quad R_a(v, h, i, j, k) := \begin{pmatrix} R_{a\_x}(v, h, i, j, k) \\ R_{a\_y}(v, h, i, j, k) \\ R_{a\_z}(v, h, i, j, k) \end{pmatrix}$$

Lower Hemisphere cartesian coordinates for active resultant

$$X_0(v, h, i, j, k) := \frac{R_{rc} \cdot r_{a\_x}(v, h, i, j, k)}{1 - r_{a\_z}(v, h, i, j, k)} \quad Y_0(v, h, i, j, k) := \frac{R_{rc} \cdot r_{a\_y}(v, h, i, j, k)}{1 - r_{a\_z}(v, h, i, j, k)}$$

For block normals

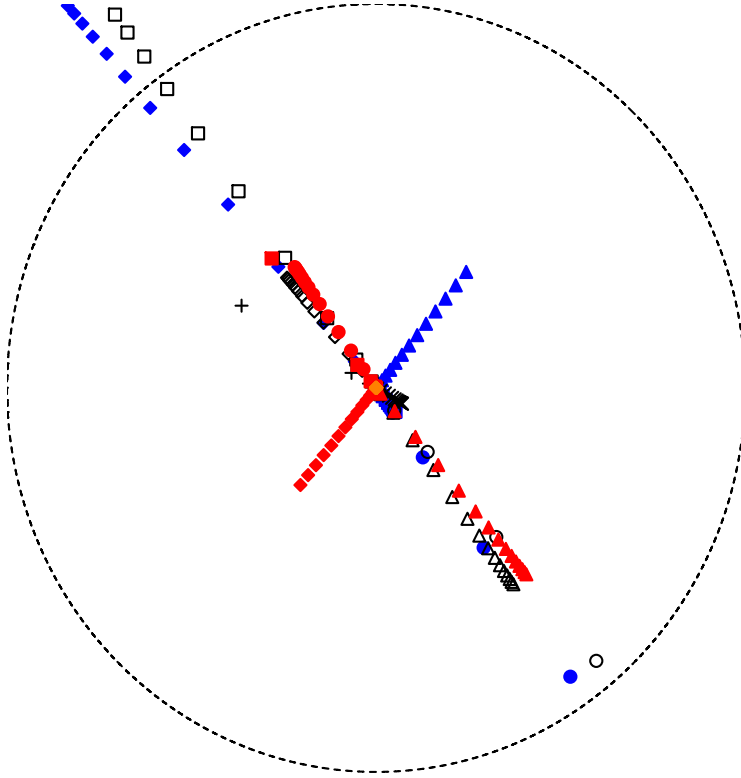
$$X_n(n_b, i) := \frac{R_{rc} \cdot \left( n_b^{(i)} \right)_1}{1 - \left( n_b^{(i)} \right)_3} \quad Y_n(n_b, i) := \frac{R_{rc} \cdot \left( n_b^{(i)} \right)_2}{1 - \left( n_b^{(i)} \right)_3}$$

Plot of active resultant paths

$K := 1$

$v := 0 \frac{m}{s}, 1 \frac{m}{s} .. 15 \frac{m}{s}$       Range of applicable flow velocities

Lower Hemisphere Stereonet



----- Ref. Circle

- ◆◆◆ J1
- J2
- ▲▲▲ J3
- ■ ■ F
- +++ J1 J2
- J1 J3
- ◇◇◇ J1 F
- J2 J3
- △△△ J2 F
- ××× J3 F
- ■ ■ J1 J2 J3
- ◆◆◆ J1 J2 F
- J1 J3 F
- ▲▲▲ J2 J3 F
- ◆◆◆ J1 J2 J3 F

# KINEMATICS

## Lifting

Criteria - Resultant plots inside the JP for the removable block (UH stereonet, Lower focal point projection)

$$r_a * n_b > 0 \quad \text{for all joint planes} \quad \text{Goodman \& Shi (1985) - Pg. 305}$$

Function for determining when lifting occurs as a function of flow velocity.

$$F_l(v, h, i, j, k) := \begin{cases} \sqrt{R_{a_x}(v, h, i, j, k)^2 + R_{a_y}(v, h, i, j, k)^2 + R_{a_z}(v, h, i, j, k)^2} & \text{if } (r_a(v, h, i, j, k) \cdot n_b^{(1)} > 0) \wedge (r_a(v, h, i, j, k) \cdot n_b^{(2)} > 0) \wedge (r_a(v, h, i, j, k) \cdot n_b^{(3)} > 0) \\ -99999N & \text{otherwise} \end{cases}$$

## Sliding 1-Plane

Sliding direction

$$s_1(v, h, i, j, k) := \frac{\left( n^{(1)} \times R_a(v, h, i, j, k) \right) \times n^{(1)}}{\left| n^{(1)} \times R_a(v, h, i, j, k) \right|} \quad \text{Plane 1}$$

$$s_2(v, h, i, j, k) := \frac{\left( n^{(2)} \times R_a(v, h, i, j, k) \right) \times n^{(2)}}{\left| n^{(2)} \times R_a(v, h, i, j, k) \right|} \quad \text{Plane 2}$$

$$s_3(v, h, i, j, k) := \frac{\left( n^{(3)} \times R_a(v, h, i, j, k) \right) \times n^{(3)}}{\left| n^{(3)} \times R_a(v, h, i, j, k) \right|} \quad \text{Plane 3}$$

Criteria 1)  $n_b * R_a \leq 0$ , where  $n_b$  is the blockside normal (i.e., the normal pointing into the block)

$$2) s_i * n_{bj} > 0 \quad \text{for all } i \text{ not equal to } j \quad \text{Goodman \& Shi (1985) - Pg. 305}$$

Equations for the fictitious required resisting force for sliding on 1 plane

$$F1(v, \phi, h, i, j, k) := \begin{cases} \left| \left( n^{(1)} \times R_a(v, h, i, j, k) \right) \right| - \left| n^{(1)} \cdot R_a(v, h, i, j, k) \right| \cdot \tan(\phi) & \text{if } (n_b^{(1)} \cdot R_a(v, h, i, j, k) \leq 0) \wedge (s_1(v, h, i, j, k) \cdot n_b^{(2)} > 0) \wedge (s_1(v, h, i, j, k) \cdot n_b^{(3)} > 0) \\ -99999N & \text{otherwise} \end{cases}$$

$$F2(v, \phi, h, i, j, k) := \begin{cases} \left| \left( n^{(2)} \times R_a(v, h, i, j, k) \right) \right| - \left| n^{(2)} \cdot R_a(v, h, i, j, k) \right| \cdot \tan(\phi) & \text{if } (n_b^{(2)} \cdot R_a(v, h, i, j, k) \leq 0) \wedge (s_2(v, h, i, j, k) \cdot n_b^{(1)} > 0) \wedge (s_2(v, h, i, j, k) \cdot n_b^{(3)} > 0) \\ -99999N & \text{otherwise} \end{cases}$$

$$F3(v, \phi, h, i, j, k) := \begin{cases} \left| \left( n^{(3)} \times R_a(v, h, i, j, k) \right) \right| - \left| n^{(3)} \cdot R_a(v, h, i, j, k) \right| \cdot \tan(\phi) & \text{if } (n_b^{(3)} \cdot R_a(v, h, i, j, k) \leq 0) \wedge (s_3(v, h, i, j, k) \cdot n_b^{(1)} > 0) \wedge (s_3(v, h, i, j, k) \cdot n_b^{(2)} > 0) \\ -99999N & \text{otherwise} \end{cases}$$

## Sliding 2-Plane

Sliding Direction (for known resultant)

$$s_{12}(v, h, i, j, k) := \frac{n^{(1)} \times n^{(2)}}{|n^{(1)} \times n^{(2)}|} \cdot \text{sign} \left[ \left( n^{(1)} \times n^{(2)} \right) \cdot R_a(v, h, i, j, k) \right]$$

$$s_{13}(v, h, i, j, k) := \frac{n^{(1)} \times n^{(3)}}{|n^{(1)} \times n^{(3)}|} \cdot \text{sign} \left[ \left( n^{(1)} \times n^{(3)} \right) \cdot R_a(v, h, i, j, k) \right]$$

$$s_{23}(v, h, i, j, k) := \frac{n^{(2)} \times n^{(3)}}{|n^{(2)} \times n^{(3)}|} \cdot \text{sign} \left[ \left( n^{(2)} \times n^{(3)} \right) \cdot R_a(v, h, i, j, k) \right]$$

Criteria (sliding on plane ij) - Goodman & Shi (1985) - Pg. 305

- 1)  $s_{ij} * n_{bk} > 0$ , and
- 2)  $s_i * n_{bj} \leq 0$ , and
- 3)  $s_j * n_{bi} \leq 0$

Equations for the fictitious required resisting force for sliding on 2-planes

$$F_{12}(v, \phi, h, i, j, k) := \begin{cases} \frac{\left[ \left| R_a(v, h, i, j, k) \cdot \left( n^{(1)} \times n^{(2)} \right) \cdot |n^{(1)} \times n^{(2)}| - \left[ \left( R_a(v, h, i, j, k) \times n^{(2)} \right) \cdot \left( n^{(1)} \times n^{(2)} \right) \right] \cdot \tan(\phi) - \left[ \left( R_a(v, h, i, j, k) \times n^{(1)} \right) \cdot \left( n^{(1)} \times n^{(2)} \right) \right] \cdot \tan(\phi) \right|}{\left( |n^{(1)} \times n^{(2)}| \right)^2} & \text{if } \left( s_{12}(v, h, i, j, k) \cdot n_b^{(3)} > 0 \right) \wedge \left( s_1(v, h, i, j, k) \cdot n_b^{(2)} \leq 0 \right) \wedge \left( s_2(v, h, i, j, k) \cdot n_b^{(1)} \leq 0 \right) \\ (-99999\text{N}) \text{ otherwise} & \end{cases}$$

$$F_{13}(v, \phi, h, i, j, k) := \begin{cases} \frac{\left[ \left| R_a(v, h, i, j, k) \cdot \left( n^{(1)} \times n^{(3)} \right) \cdot |n^{(1)} \times n^{(3)}| - \left[ \left( R_a(v, h, i, j, k) \times n^{(3)} \right) \cdot \left( n^{(1)} \times n^{(3)} \right) \right] \cdot \tan(\phi) - \left[ \left( R_a(v, h, i, j, k) \times n^{(1)} \right) \cdot \left( n^{(1)} \times n^{(3)} \right) \right] \cdot \tan(\phi) \right|}{\left( |n^{(1)} \times n^{(3)}| \right)^2} & \text{if } \left( s_{13}(v, h, i, j, k) \cdot n_b^{(2)} > 0 \right) \wedge \left( s_1(v, h, i, j, k) \cdot n_b^{(3)} \leq 0 \right) \wedge \left( s_3(v, h, i, j, k) \cdot n_b^{(1)} \leq 0 \right) \\ (-99999\text{N}) \text{ otherwise} & \end{cases}$$

$$F_{23}(v, \phi, h, i, j, k) := \begin{cases} \frac{\left[ \left| R_a(v, h, i, j, k) \cdot \left( n^{(2)} \times n^{(3)} \right) \cdot |n^{(2)} \times n^{(3)}| - \left[ \left( R_a(v, h, i, j, k) \times n^{(3)} \right) \cdot \left( n^{(2)} \times n^{(3)} \right) \right] \cdot \tan(\phi) - \left[ \left( R_a(v, h, i, j, k) \times n^{(2)} \right) \cdot \left( n^{(2)} \times n^{(3)} \right) \right] \cdot \tan(\phi) \right|}{\left( |n^{(2)} \times n^{(3)}| \right)^2} & \text{if } \left( s_{23}(v, h, i, j, k) \cdot n_b^{(1)} > 0 \right) \wedge \left( s_2(v, h, i, j, k) \cdot n_b^{(3)} \leq 0 \right) \wedge \left( s_3(v, h, i, j, k) \cdot n_b^{(2)} \leq 0 \right) \\ (-99999\text{N}) \text{ otherwise} & \end{cases}$$

Plot of required stabilizing force for all applicable failure modes

$$v := 0 \frac{\text{m}}{\text{s}}, 0.2 \frac{\text{m}}{\text{s}} .. 15 \frac{\text{m}}{\text{s}}$$

